

Ballistic Transport at Uniform Temperature

Nawaf Bou-Rabee*

Houman Owhadi*

17 February 2013

Abstract

A paradigm for isothermal, mechanical rectification of stochastic fluctuations is introduced in this paper. The central idea is to transform energy injected by random perturbations into rigid-body rotational kinetic energy. The prototype considered in this paper is a mechanical system consisting of a set of rigid bodies in interaction through magnetic fields. The system is stochastically forced by white noise and dissipative through mechanical friction. The Gibbs-Boltzmann distribution at a specific temperature defines the unique invariant measure under the flow of this stochastic process and allows us to define “the temperature” of the system. This measure is also ergodic and strongly mixing. Although the system does not exhibit global directed motion, it is shown that global ballistic motion is possible (the mean-squared displacement grows like t^2). More precisely, although work cannot be extracted from thermal energy by the second law of thermodynamics, it is shown that ballistic transport from thermal energy is possible. In particular, the dynamics is characterized by a meta-stable state in which the system exhibits directed motion over random time scales. This phenomenon is caused by interaction of three attributes of the system: a non flat (yet bounded) potential energy landscape, a rigid body effect (coupling translational momentum and angular momentum through friction) and the degeneracy of the noise/friction tensor on the momentums (the fact that noise is not applied to all degrees of freedom).

1 Introduction

Mechanical rectification was introduced to describe devices that convert small-amplitude mechanical vibrations into directed rotary or rectilinear mechanical motion [6]. The purpose of this paper is to extend this concept to mechanical systems in isothermal environments subjected to stochastic fluctuations. Although the second law of thermodynamics prevents directed mechanical motion from thermal fluctuations in an isothermal environment, violations of the second law of thermodynamics on certain time-scales in microscopic systems have been theoretically predicted [10; 12] and experimentally observed [7; 20].

In this paper we exhibit a system characterized by ballistic non-directed motion at uniform temperature. Set μ to be the unique invariant measure of the system and $x(t)$ the displacement of the system at time t then μ a.s. $\lim_{t \rightarrow \infty} (x(t) - x(0))/t \rightarrow 0$ but $\mathbb{E}_\mu[\{x(t) - \mathbb{E}(x(t))\}^2] \sim t^2$. Moreover the system is characterized by “dynamic” meta-stable states in which it experiences ballistic directed motion over random time scales (flights) in addition to “static” meta-stable states where the system is “captured” in potential wells.

The mechanism introduced in this paper is different from the one associated to the Gallavotti-Cohen fluctuation theorem [10]. It is based on the fact that one can obtain anomalous diffusion by introducing degenerate noise and friction in the momentums. This

*Applied & Computational Mathematics (ACM), Caltech, Pasadena, CA 91125 (nawaf@acm.caltech.edu, owhadi@acm.caltech.edu).

anomalous diffusion manifests itself in the just mentioned flights over time-scales which are random and the probability distributions of the flight-durations have a heavy tail. Moreover we expect that it will be of relevance to Brownian motors [2; 19] since it shows how thermal noise can be used to get ballistic transport, in other words how to obtain fast and efficient intracellular transport without using chemical energy. Although global ballistic transport is achieved it is not directed and hence work is not produced from thermal fluctuations (this mechanism is not in violation of the second law of thermodynamics). However this mechanism would be sufficient for intracellular transport of a large fraction of the material being carried to target areas with ballistic speed without draining cellular energy reserves.

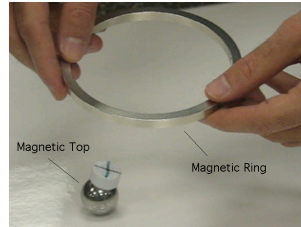


Figure 1.1: **Picture of mechanical system.** The physical system consists of a magnetized axisymmetric top on a flat surface and a magnetized ring as shown above. The dipole moments in the ring are oriented radially.

The prototype analyzed in this paper consists of a magnetized top (ball) on a surface interacting with a suspended magnetized ring as shown in Fig. 1.1. The following dynamics is observed: when one lowers the magnetic ring to within a certain range of heights and then tilts the ring, one observes the top transition from a state of no spin about its axis of symmetry to a state of nonzero spin. The reader is referred to the following urls for movies and simulations of the phenomenon:

<http://www.acm.caltech.edu/~nawaf/BallisticTransport/>

<http://www.acm.caltech.edu/~owhadi/BallisticTransport/>

This phenomenon seems counterintuitive and non-Hamiltonian, since one would expect the angular momentum of the top to be conserved (since without friction the Hamiltonian of the system is invariant under an S^1 rotation of the ball). The origin of this mechanical device can be traced back to the work of David Hamel on magnetic motors in the unofficial sub-scene of physics [15]. The mechanism presented in this paper when the device is not at uniform temperature could in principle be used as a method of extracting energy from macroscopic fluctuations.

2 Preview of the Paper

In section 4 Hamel's device is analyzed through an idealized model based on magnetostatics and the spinning of the top is caused by the introduction of surface frictional forces. Simulations (figure 1.2) are done using variational integrators and concur with experimental observations.

In section 5 the magnetic ring is allowed to be dynamic, and a fixed outer ring of a finite number of magnetic dipoles is introduced to stabilize it (see figure 5.1). The inner magnetic ring is excited through white noise applied as a torque. The steel ball and inner ring are coupled through a magnetostatic potential and the motion of the steel ball is dissipative through slip friction.

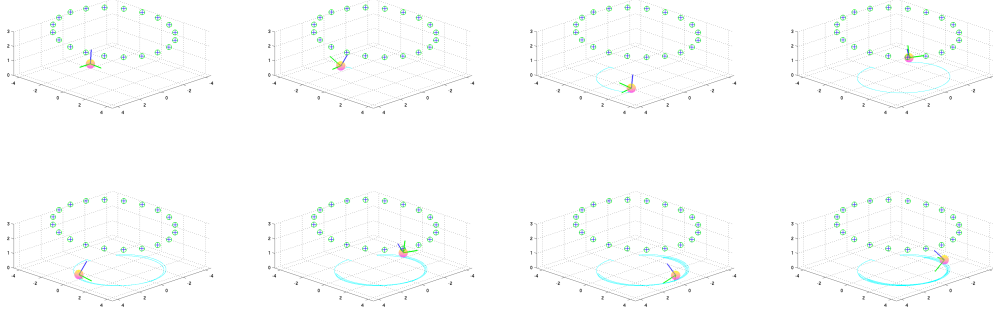


Figure 1.2: **Snapshots of Nonconservative Tilted Simulation.** The above are snapshots of the simulation described in Fig. 4.9. The top is initially set with its axis of symmetry pointing nearly vertical. The axis of symmetry then aligns with the ambient magnetic field. However, the state is not a minimum of V_e , and hence, the state is unstable. The top moves towards a state that minimizes its magnetic potential energy, and acquires spin in this process.

The mathematical description of the fluctuation driven motor is obtained by generalizing Langevin processes from a system of particles on a linear configuration space to rigidified particles whose configuration space is the Lie group $SE(3)$. The question of random perturbations of a rigid body was treated by previous investigators who added perturbations to the Lie-Poisson equations without potential or dissipative torques [13; 14]. Hence, they do not consider generalizing Langevin processes to the Lie-Poisson setting.

We refer to figure 2.1 for a plot of the angular position of the ball versus time for different values of noise amplitude α . The simulation of the system exhibits two distinct kinds of metastable states. In the first kind the ball is “stuck” in a magnetic potential well whose depth depends on the position of the inner ring, and moves into another potential well when the energy barrier between the two wells is close to minimum (a phenomenon known as stochastic resonance) or transitions to a metastable state of the second kind. In the second kind the ball spins in circles clockwise or counter-clockwise in a directed way for a random amount of time (that numerically and heuristically observe to be exponential in law) until it gets stuck in a potential well.

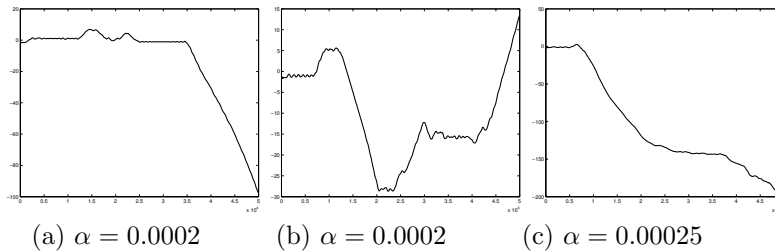


Figure 2.1: **Angular-position of magnetic ball (non-uniform temperature).** The angular component of the center of mass is plotted for three different realizations. The plots show the magnetic ball transition between two meta-stable states: noise-driven and inertia-driven motion.

Since the system associated to figure 2.1 is described by a generalized Langevin process it is possible to introduce a notion of temperature defined as $\frac{(\text{noise amplitude})^2}{\text{friction constant}}$. However, since noise but no friction is applied at the level of the inner ring and friction but no noise

is applied at the level of the ball, the system is not at uniform temperature, i.e., the inner ring is at infinite temperature and the ball is at zero temperature. Nevertheless, one could in principle use such a mechanism as a way to extract energy from macroscopic fluctuations.

In a second step frictional torque is introduced to the inner ring and thermal torque (white noise) to the ball, so that the generator of the process is characterized by a unique Gibbs-Boltzmann invariant distribution. Throughout this paper we interpret this property as placing the mechanical system at uniform temperature. We refer to figure 2.2 for a plot of the angular position of the ball versus time for different values of noise amplitude α (and temperature). The system is still characterized by ballistic directed motion meta-stable states.

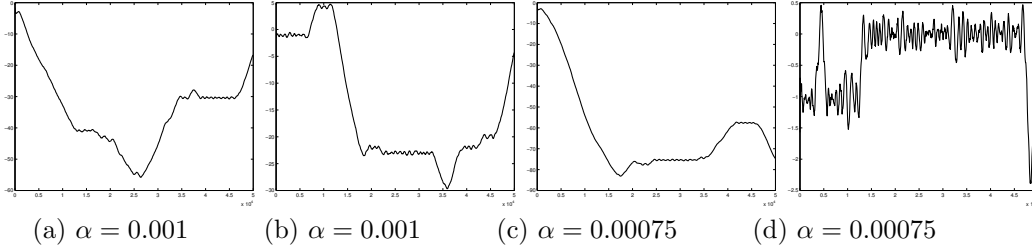


Figure 2.2: **Angular-position of magnetic ball (uniform temperature).** Four different realizations of the angular component of the center of mass are plotted. The plots for $\alpha = 0.0002$ show the magnetic ball transition between two metastable states: noise-driven and inertia-driven motion. If α is increased to $\alpha = 0.00025$, realization (c) shows a similar transition. Realization (d), however, does not show such a transition, i.e., the ball never transitions to a metastable state of the second kind.

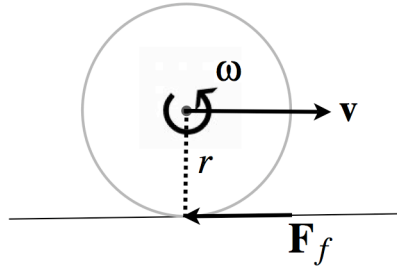


Figure 2.3: **Sliding Disk.** Consider a sliding disk of radius r that is free to translate and rotate on a surface. We assume the disk is in sliding frictional contact with the surface. The configuration space of the system is $SE(2)$, but with the surface constraint the configuration space is just $\mathbb{R} \times SO(2)$.

To understand the behavior of the fluctuation driven motor prototype, the paper considers in section 3 a sliding disk (figure 2.3) that has the same essential behavior, but whose configuration space is $SE(2)$. The solution of this simplified system is a Langevin process with degenerate noise and friction matrices in the momentums. The disk is free to slide and rotate. Assume that one rescales position by r and time by some characteristic frequency of rotation or other time-scale. The dimensionless Lagrangian is given by the difference of kinetic and potential energy

$$L(x, v, \theta, \omega) = \frac{1}{2}v^2 + \frac{\sigma}{2}\omega^2 - U(x)$$

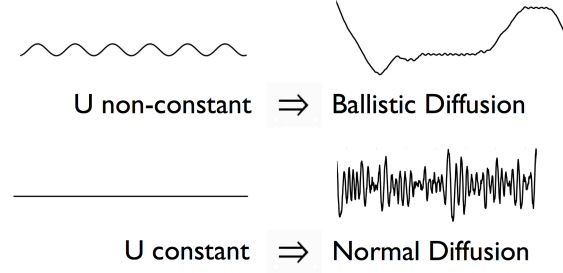


Figure 2.4: **Ballistic vs. Normal Diffusion.** If U is non-constant theorem 3.1 implies that the mean squared displacement with respect to the invariant law is ballistic. Numerically, flights are observed in the x -displacement as shown in the diagram. However, if U is constant this diffusion is normal, i.e., the x -displacement behaves like Brownian motion.

where $U : \mathbb{R} \rightarrow \mathbb{R}$ is assumed to be smooth and periodic. If $U = \cos(x)$, figure 2.5 shows that the sliding disk is a modified one-dimensional pendulum. The contact with the surface is modelled using a sliding friction law. For this purpose we introduce a symmetric matrix \mathbf{C} defined as,

$$\mathbf{C} = \begin{bmatrix} 1 & 1/\sigma \\ 1/\sigma & 1/\sigma^2 \end{bmatrix}.$$

\mathbf{C} is degenerate since the frictional force is actually applied to only a single degree of freedom, and hence, one of its eigenvalues is zero. In addition to friction the system is excited by white noise so that the governing equations become

$$\begin{cases} dx = v dt \\ d\theta = \omega dt \\ \begin{bmatrix} dv \\ d\omega \end{bmatrix} = \begin{bmatrix} -\partial_x U \\ 0 \end{bmatrix} dt - c \mathbf{C} \begin{bmatrix} v \\ \sigma \omega \end{bmatrix} dt + \alpha \mathbf{C}^{1/2} \begin{bmatrix} dB_v \\ dB_\omega \end{bmatrix} \end{cases} \quad (2.1)$$

where $\mathbf{C}^{1/2}$ is the matrix square root of \mathbf{C} . Let E denote the energy of the mechanical system given by,

$$E = \frac{1}{2}v^2 + \frac{1}{2}\sigma\omega^2 + U(x), \quad (2.2)$$

and let $\beta = 2c/\alpha^2$.

In [4], we show that the Gibbs-Boltzmann distribution

$$\mu = \exp(-\beta E),$$

defines the unique invariant measure under the flow of the sliding disk. This measure is also ergodic and strongly mixing. Using this result we prove in § 3, that if U is non-constant then the x -displacement of the sliding disk is μ a.s. not ballistic (cf. proposition 3.2). However, the mean-squared displacement with respect to the invariant law is ballistic (cf. theorem 3.1). More precisely, we show that the squared standard deviation of the x -displacement with respect to its noise-average grows like t^2 . This implies that the process exhibits not only ballistic transport but also ballistic diffusion. If U is constant then the squared standard deviation of the x -displacement is diffusive (grows like t).

In the numerics the *sliding disk is initially at rest* and averages are computed with respect to realizations. Numerically one observes the following consequences of this ballistic

behavior. Figure 2.6 shows that when U is non-constant then the motion is characterized by meta-stable directed motion states. Figure 2.7 shows that the mean square displacement $\mathbb{E}[x(t)^2]$ grows like t (with respect to time) when U is constant or in the case of a one dimensional standard Langevin process (control) whereas it grows like t^2 as soon as U is non-constant (the motion becomes ballistic). A diagram comparing the solution behavior in the U constant and non-constant cases is provided in Figure 2.4. Figure 2.8 corresponds to the plot of

$$\frac{\text{Cov}(x(t+2s) - x(t+s), x(t+s) - x(t))}{(\text{Var}(x(t+2s) - x(t+s)))^{\frac{1}{2}} (\text{Var}(x(t+s) - x(t)))^{\frac{1}{2}}} \quad (2.3)$$

for t large as a function of s . It clearly shows that the system is characterized by long time memory/correlation when U is non-constant whereas it has almost no memory when U is constant or in the case of a one dimensional standard Langevin process.

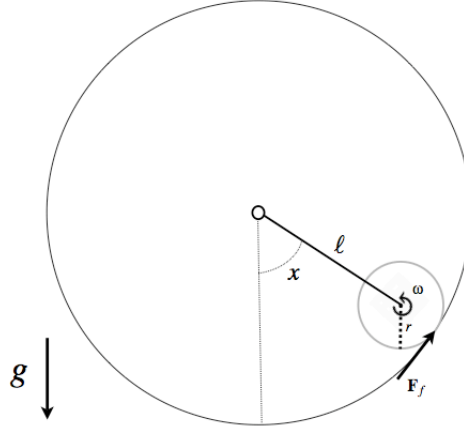


Figure 2.5: **Ballistic Pendulum.** If the dimensionless potential is $U = \cos(x)$, then the sliding disk is simply a pendulum in which the bob in the pendulum is replaced by a disk and the pendulum is placed within a cylinder as shown.

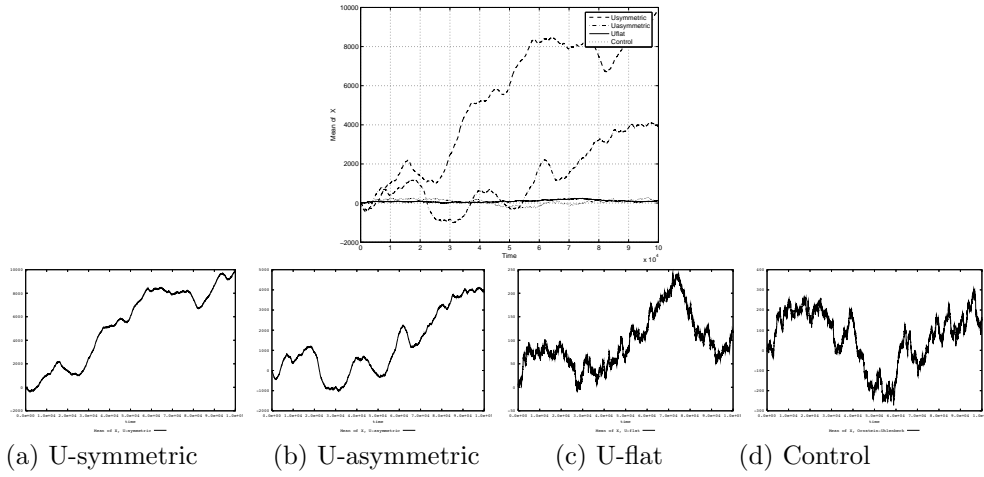


Figure 2.6: **Sliding Disk at Uniform Temperature**, $h = 0.01$, $\alpha = 5.0$, $c = 0.1$. The mean of the x -displacement of the disk for U symmetric, asymmetric, flat and control case. Figures (a) and (b) show that when U is non-constant, directed motion as a meta-stable state is possible. On the other hand, (c) and (d) do not show such behavior. The figure on the top superposes these graphs in a single plot for comparison.

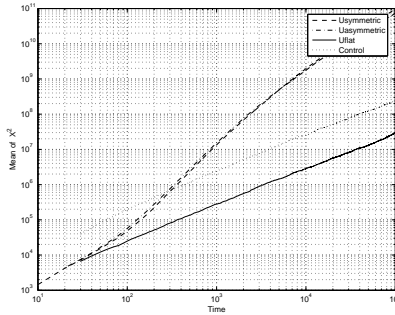


Figure 2.7: **Sliding Disk at Uniform temperature**, $h = 0.01$, $\alpha = 5.0$, $c = 0.1$. A log-log plot of the mean squared displacement of the ball. It clearly shows that the x -position exhibits anomalous diffusion when U is symmetric or asymmetric. In the control and flat U cases the diffusion is normal.

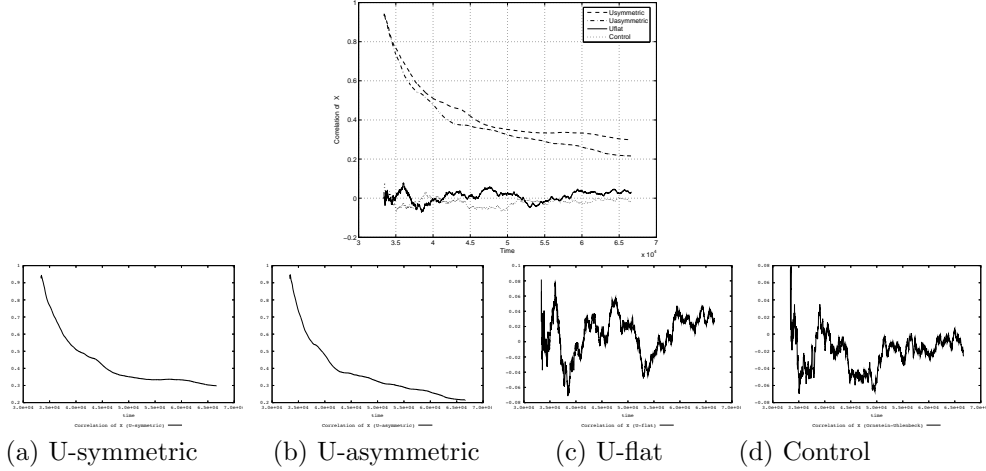


Figure 2.8: **Sliding Disk at Uniform Temperature**, $h = 0.01$, $\alpha = 5.0$, $c = 0.1$. The correlation of the x displacement of the disk for U symmetric, asymmetric, flat, and the control case. When U is symmetric or asymmetric the correlation in the x displacement is nonzero for a certain time-scale which is larger than the characteristic time-scales associated with U and with the friction factor. However, in the other cases the correlation is negligible. The figure on the top superposes these graphs in a single plot for comparison.

3 Sliding Disk: Simplified Model

To understand the behavior of the prototype stochastic mechanical rectifier which will be treated in detail in subsequent sections, we designed a simplified model whose configuration space is $SE(2)$. The system consists of a disk sliding on a surface as shown in Figure 2.3. The effect of the outer ring is modelled as a periodic, one-dimensional potential; while the effect of the inner ring is incorporated into white noise. The SDE for the isothermal, sliding disk is a Langevin process, but the noise and friction matrices are degenerate. A statistical numerical analysis discussed below shows that this process has two interesting statistical properties which are both linked to rigid-body inertial effects: 1) a non-trivial correlation on certain time-scales and 2) ballistic diffusion.

Ballistic Transport at Uniform Temperature The proof that the sliding disk is at uniform temperature is based on finding the generator for (2.1) and showing that the Gibbs measure is the unique, invariant measure under the flow of this generator.

Theorem 3.1. *Let $\chi := \mathbb{T} \times \mathbb{R} \times \mathbb{T} \times \mathbb{R}$ denote the phase space of the sliding disk (\mathbb{T} standing for the torus of dimension one). Set $\xi := (x, v, \theta, \omega)$ to be the solution of (2.1). Let E denote the energy of the sliding disk given by, $E = \frac{1}{2}v^2 + \frac{1}{2}\sigma\omega^2 + U(x)$. Set $\beta = 2c/\alpha^2$ and let μ be the Gibbs probability measure defined by*

$$\mu(d\xi) := \frac{e^{-\beta E}}{Z} d\xi \quad (3.1)$$

where $Z := \int_{\chi} e^{-\beta E} d\xi$. If U is non-constant, then the Gibbs measure μ is ergodic and strongly mixing with respect to the stochastic process ξ . Furthermore, it is the unique, invariant probability measure for the stochastic process ξ .

This result is a special case of the proof provided in [4]. To determine the measure is invariant, one computes the infinitesimal generator \mathcal{L} associated to the stochastic process ξ

and proves that if f is μ - measureable then,

$$\int_{\chi} \mathcal{L}f \mu(d\xi) = 0$$

Using the fact that the measure is ergodic, one can readily prove that the x -displacement itself is not ballistic.

Proposition 3.2. *Provided that U is non-constant, then μ a.s.*

$$\lim_{t \rightarrow \infty} \frac{x(t) - x(0)}{t} \rightarrow 0.$$

Proof. Since μ is ergodic with respect to ξ ,

$$\lim_{t \rightarrow \infty} \frac{x(t) - x(0)}{t} = \lim_{t \rightarrow \infty} \frac{1}{t} \int_0^t v dt = \int_{\chi} v \mu(d\xi) = 0.$$

■

Moreover, as stated in the following proposition, the squared standard deviation of the $x + \theta$ -degree of freedom of the sliding disk grows like t . Let \mathbb{E} denote the expectation with respect to the Brownian noise and \mathbb{E}_{μ} the expectation with respect to the Brownian noise and the initial configuration (sampled from the invariant measure μ). Set $x_t = x(t)$ and $\theta_t = \theta(t)$.

Proposition 3.3. *The squared standard deviation of the $x_t + \theta_t$ -degree of freedom is diffusive, i.e.,*

$$\lim_{t \rightarrow \infty} \frac{\mathbb{E}_{\mu}[(x_t + \theta_t - \mathbb{E}[x_t + \theta_t])^2]}{t} = \frac{2\alpha^2\sigma^2}{c^2(\sigma^2 + 1)}. \quad (3.2)$$

Proof. First, diagonalize the diffusion and friction matrices in (2.1) using the following invertible matrix:

$$\mathbf{V} = \frac{1}{1 + \sigma} \begin{bmatrix} -1 & \sigma \\ 1 & 1 \end{bmatrix}$$

as follows,

$$\mathbf{V} \begin{bmatrix} dv \\ d\omega \end{bmatrix} = \mathbf{V} \begin{bmatrix} -\partial_x U \\ 0 \end{bmatrix} dt - c \begin{bmatrix} 0 & 0 \\ 0 & \frac{\sigma+1}{\sigma} \end{bmatrix} \mathbf{V} \begin{bmatrix} v \\ \omega \end{bmatrix} dt + \frac{\alpha(\sigma+1)}{\sqrt{\sigma^2+1}} \begin{bmatrix} 0 & 0 \\ 0 & 1 \end{bmatrix} \mathbf{V} \begin{bmatrix} dB_v \\ dB_{\omega} \end{bmatrix}.$$

Simplifying this expression yields the following pair of equations:

$$d(-v + \sigma\omega) = \partial_x U dt, \quad (3.3)$$

$$d(v + \omega) = -\partial_x U dt - c\gamma(v + \omega) + \bar{\alpha}(dB_v + dB_{\omega}). \quad (3.4)$$

where

$$\gamma = \frac{(\sigma+1)}{\sigma}, \quad \bar{\alpha} = \frac{\alpha(\sigma+1)}{\sqrt{\sigma^2+1}}.$$

Set $B_s := (B_v + B_{\omega})/\sqrt{2}$. Integrating (3.3) and (3.4) gives

$$-v + \sigma\omega = -v_0 + \sigma\omega_0 + \int_0^t \partial_x U ds, \quad (3.5)$$

$$v + \omega = (v_0 + \omega_0)e^{-c\gamma t} - \int_0^t e^{-c\gamma(t-s)} \partial_x U ds + \sqrt{2}\bar{\alpha} \int_0^t e^{-c\gamma(t-s)} dB_s. \quad (3.6)$$

Integrating (3.6) gives

$$(x_t + \theta_t) - (x_0 + \theta_0) = \frac{v_0 + \omega_0}{c\gamma} (1 - e^{-c\gamma t}) - \int_0^t \frac{1 - e^{-c\gamma(t-s)}}{c\gamma} \partial_x U ds \\ + \sqrt{2\bar{\alpha}} \int_0^t \frac{1 - e^{-c\gamma(t-s)}}{c\gamma} dB_s.$$

The result follows by observing that

$$\int_0^t \partial_x U ds = (-v_t + \sigma\omega_t) - (-v_0 + \sigma\omega_0) \quad (3.7)$$

■

However, one can prove that the squared standard deviation of the $-x_t + \sigma\theta_t$ -degree of freedom grows like t^2 . This implies that the process exhibits not only ballistic transport but also ballistic diffusion along this degree of freedom.

Proposition 3.4. *Assume that U is non constant, then*

$$\limsup_{t \rightarrow \infty} \frac{\mathbb{E}_\mu \left[\left(-x_t + \sigma\theta_t - \mathbb{E}[-x_t + \sigma\theta_t] \right)^2 \right]}{t^2} \leq 4 \frac{1 + \sigma}{\beta} \quad (3.8)$$

and

$$\liminf_{t \rightarrow \infty} \frac{\mathbb{E}_\mu \left[\left(-x_t + \sigma\theta_t - \mathbb{E}[-x_t + \sigma\theta_t] \right)^2 \right]}{t^2} \geq \frac{1}{4} \frac{1 + \sigma}{\beta} \quad (3.9)$$

Proof. From Cauchy-Schwartz inequality one obtains that

$$\left(\frac{1}{t} \int_0^t (-v_s + \sigma\omega_s) ds \right)^2 \leq \frac{1}{t} \int_0^t (-v_s + \sigma\omega_s)^2 ds.$$

Hence

$$\limsup_{t \rightarrow \infty} \frac{\mathbb{E}_\mu \left[\left(-x_t + \sigma\theta_t - (-x_0 + \sigma\theta_0) \right)^2 \right]}{t^2} \leq \mu[(-v_0 + \sigma\omega_0)^2]. \quad (3.10)$$

We obtain the first inequality of the proposition by observing that

$$\mu[(-v_0 + \sigma\omega_0)^2] = \frac{1 + \sigma}{\beta}.$$

and

$$\mathbb{E}_\mu \left[\left(\mathbb{E}[-x_t + \sigma\theta_t] - (-x_0 + \sigma\theta_0) \right)^2 \right] \leq \mathbb{E}_\mu \left[\left(-x_t + \sigma\theta_t - (-x_0 + \sigma\theta_0) \right)^2 \right] \quad (3.11)$$

Let us now prove the lower bound. Integrating equation (3.5) gives

$$-x_t + \sigma\theta_t - \mathbb{E}[-x_t + \sigma\theta_t] = t \int_0^t \left(1 - \frac{s}{t} \right) (\partial_x U - \mathbb{E}[\partial_x U]) ds \quad (3.12)$$

Write

$$A_t = \int_0^t \left(1 - \frac{s}{t} \right) (\partial_x U - \mathbb{E}[\partial_x U]) ds \quad (3.13)$$

and

$$B_t = \int_0^t \frac{s}{t} (\partial_x U - \mathbb{E}[\partial_x U]) ds \quad (3.14)$$

Observe that

$$A_t + B_t = (-v_t + \sigma\omega_t) - \mathbb{E}[-v_t + \sigma\omega_t]. \quad (3.15)$$

Since μ is strongly mixing when U is non constant, it follows that [18]

$$\liminf_{t \rightarrow \infty} \mathbb{E}_\mu[(A_t + B_t)^2] = \mu[(-v_t + \sigma\omega_t)^2] \quad (3.16)$$

Furthermore

$$\mathbb{E}_\mu[(A_t + B_t)^2] \leq 2(\mathbb{E}_\mu[A_t^2] + \mathbb{E}_\mu[B_t^2]) \quad (3.17)$$

and since the law of the process $(x_t, \theta_t, v_t, \omega_t)$ remains invariant under \mathbb{P}_μ by reversing time and flipping the velocities v_t, ω_t we deduce that $\mathbb{E}_\mu[A_t^2] = \mathbb{E}_\mu[B_t^2]$ and

$$\liminf_{t \rightarrow \infty} \mathbb{E}_\mu[A_t^2] = \frac{1}{4} \mu[(-v_t + \sigma\omega_t)^2] \quad (3.18)$$

We conclude by the taking the expectation of square of (3.12) with respect to \mathbb{E}_μ . \blacksquare

The following theorem is a straightforward consequence of the previous propositions.

Theorem 3.1. *We have*

- *If U is constant then*

$$\lim_{t \rightarrow \infty} \frac{\mathbb{E}_\mu[(x_t - \mathbb{E}[x_t])^2]}{t} = \frac{2\alpha^2\sigma^2}{c^2(\sigma^2 + 1)(\sigma + 1)^2} \quad (3.19)$$

- *If U is non constant then*

$$\limsup_{t \rightarrow \infty} \frac{\mathbb{E}_\mu[(x_t - \mathbb{E}[x_t])^2]}{t^2} \leq \frac{4}{\beta(1 + \sigma)} \quad (3.20)$$

and

$$\liminf_{t \rightarrow \infty} \frac{\mathbb{E}_\mu[(x_t - \mathbb{E}[x_t])^2]}{t^2} \geq \frac{1}{4\beta(1 + \sigma)} \quad (3.21)$$

Remark 3.1. Using Ito's formula and (2.2) one obtains that,

$$dE = -c(v + \omega)^2 dt + \frac{\alpha^2}{2} \left(1 + \frac{1}{\sigma}\right) dt + \text{martingales}.$$

Integrating this expression gives

$$E(t) - E(0) = -c \int_0^t (v + \omega)^2 ds + \frac{\alpha^2}{2} \left(1 + \frac{1}{\sigma}\right) t + \text{martingales}.$$

The first and second terms represent the energy loss due to friction and the energy injected due to the noise respectively.

Remark 3.2. Setting $v_t = v(t)$, it follows from (3.5) and (3.6) that

$$\begin{aligned} v_t = & \frac{\sigma(v_0 + \omega_0)e^{-c\gamma t} + v_0 - \sigma\omega_0}{\sigma + 1} - \int_0^t \frac{\sigma e^{-c\gamma(t-s)} + 1}{\sigma + 1} \partial_x U ds \\ & + \frac{\sqrt{2}\bar{\alpha}}{\sigma + 1} \int_0^t e^{-c\gamma(t-s)} dB_s. \end{aligned} \quad (3.22)$$

The long term memory effect exhibited in Figure 2.8 has its origin in the term $\int_0^t \partial_x U(x(s)) ds$ in (3.22). That term is equal to zero when U is constant, and itself has its origin in the rigid body interaction between rotation and translation and the fact the friction matrix is singular.

Stochastic Variational Integrator To simulate the dynamics of the sliding disk at constant temperature, a stochastic variational Euler method is applied [5]. The discrete scheme for the isothermal case is given explicitly by:

$$\begin{cases} x_{n+1} &= x_n + hv_{n+1}, \\ \theta_{n+1} &= \theta_n + h\omega_{n+1}, \\ \begin{bmatrix} v_{n+1} \\ \omega_{n+1} \end{bmatrix} &= \begin{bmatrix} v_n \\ \omega_n \end{bmatrix} + h \begin{bmatrix} -\partial_x U(x_n) \\ 0 \end{bmatrix} - hc\mathbf{C} \begin{bmatrix} v_n \\ \sigma\omega_n \end{bmatrix} + \alpha\mathbf{C}^{1/2} \begin{bmatrix} dB_v \\ dB_\omega \end{bmatrix}. \end{cases} \quad (3.23)$$

It is an explicit, first-order strongly convergent method.

Simulation We will consider four different systems to simulate. The first three are sliding disks with a symmetric, asymmetric, and flat potentials:

$U(x)$	
$\sin(x)$	symmetric
$\sin(x) + 0.4\sin(2x)$	asymmetric
0	flat

The fourth case is a control consisting of a simulation of a 1-D Langevin process at the same temperature and with a symmetric potential:

$$\begin{aligned} dX &= Vdt, \\ dV &= -cVdt - \cos(X)dt + \alpha dB_V. \end{aligned}$$

For all of the simulations the *sliding disk is initially at rest*, $r = 0.25$, $m = 1.0$, $J = mr^2/2$ and the friction and noise factors are as indicated in the figures. The means of the x displacement of the disk as shown in Fig. 2.6 are very small compared with the spread as, e.g., shown in the histogram of the final position of the ball as shown in Fig. 3.3. However, the mean squared displacement shows ballistic diffusion in the cases when U is symmetric or asymmetric and normal diffusion otherwise (see Figures 3.1-2.7). The time-scale associated with this ballistic diffusion is plotted in Fig. 2.8 which shows the correlation in the x -displacement when U is symmetric or asymmetric. This time-scale is much greater than the characteristic time-scale associated with the friction or the potential. Recall from the integral expression of the velocity, that when U is zero a rigid-body term is neglected. This demonstrates the important role of the rigid-body effect in the ballistic diffusion of the x -displacement when U is symmetric and asymmetric.

Finally we also consider adding a non-degenerate, but anisotropic dissipation matrix to the sliding disk. It is numerically observed that if the anisotropy is large enough, $\mathbb{E}(x_t^2)$ is ballistic for a long period of time.

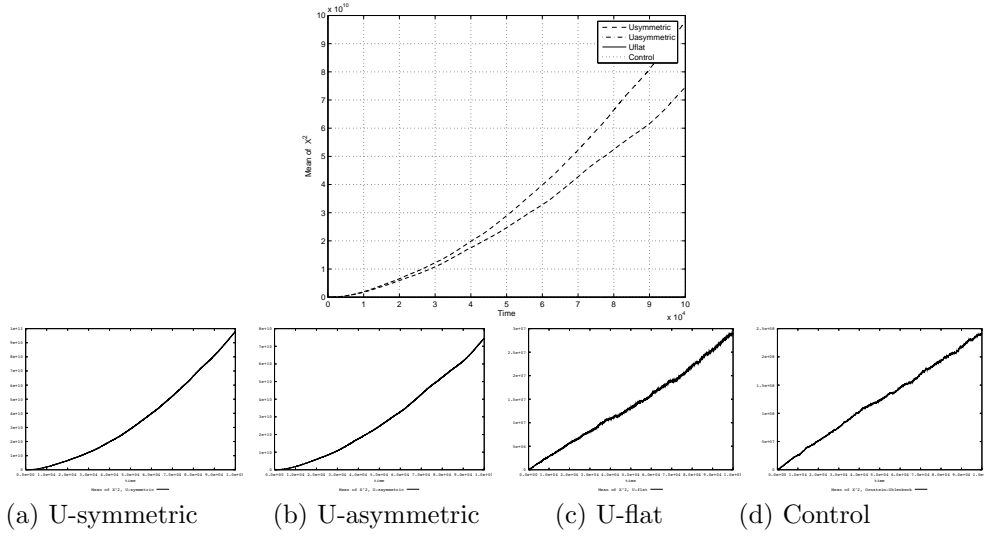


Figure 3.1: **Sliding Disk at Uniform Temperature**, $h = 0.01$, $\alpha = 5.0$, $c = 0.1$. From left: the mean squared position of the disk for U symmetric, asymmetric, flat, and the control. The figure on the top superposes these graphs in a single plot for comparison.

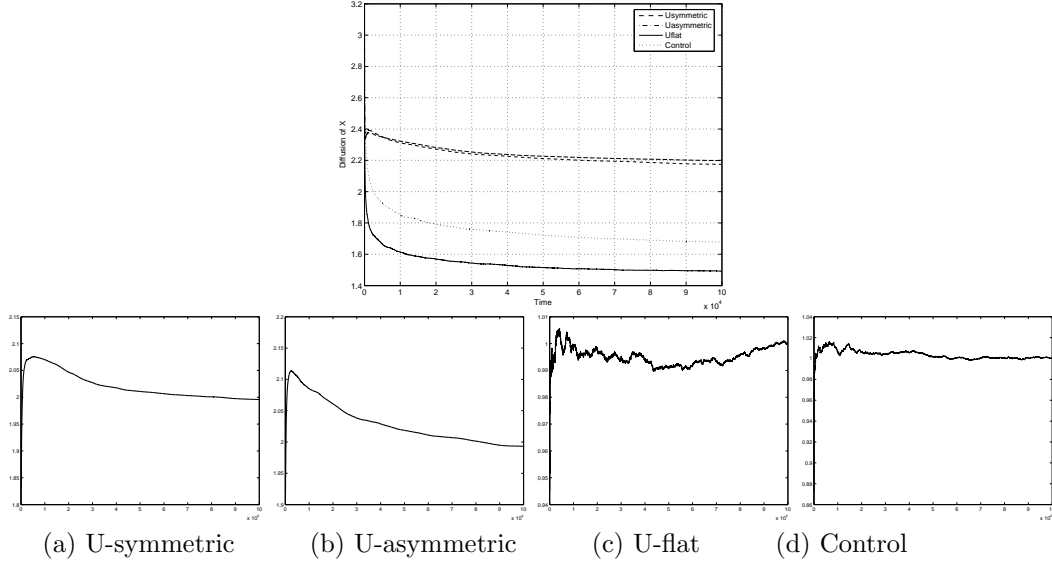


Figure 3.2: **Sliding Disk at Uniform Temperature**, $h = 0.01$, $\alpha = 5.0$, $c = 0.1$. From left: “diffusion” of x -displacement of the disk for U symmetric, asymmetric, flat, and the control. For the cases when U is flat and the control, the diffusion is normal. Whereas in the other cases the diffusion is ballistic. The figure on the top superposes these graphs in a single plot for comparison.

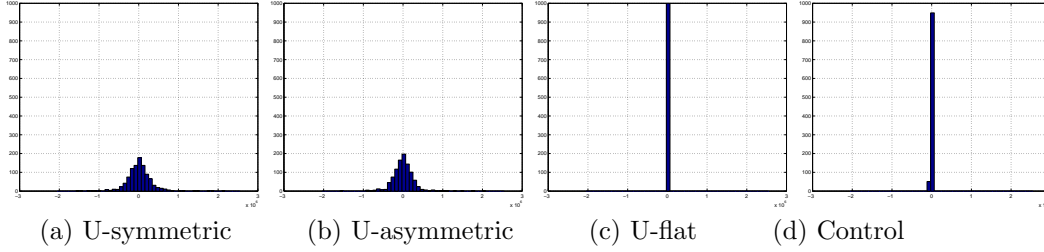


Figure 3.3: **Sliding Disk at Uniform Temperature**, $h = 0.01$, $\alpha = 5.0$, $c = 0.1$. From left: histogram of the x -displacement of the disk at $T = 50000$ for U symmetric, asymmetric, and flat. We observe a wider spread in the cases when U is symmetric or asymmetric.

4 Hamel's magnetic top

In this section an observed magnetism induced spinning phenomenon is analyzed. Up to our knowledge, the first magnetism induced spinning device was “Tesla’s egg of colombus” exhibited in 1892 [11]. Using two phase AC energizing coils in quadrature, Tesla placed a copper plated ellipsoid on a wooden plate above a rotating magnetic field. The egg stood on its pointed end without cracking its shell and began to spin at high speed to the amazement of the scientists who witnessed the experiment. This effect was caused by induced eddy currents on the surface of the ellipsoid. A related magnetism induced spinning phenomenon is the Einstein-de Hass effect in which the rotation of an object is caused by a change in magnetization [9]. In this effect the magnetic field causes an alignment of electronic spins and their angular momenta is transferred to the atomistic lattice. We will show below through an idealized model based on magnetostatics that the spinning of the top in Hamel’s device is due to surface friction.

Mechanism behind curious rotation The following observation was made on a simple mechanical system consisting of a magnetized top and ring as shown in Fig. 1.1. When the ring is held above the top within a certain range of heights, and then tilted, one observes the top transitions from a state of no spin to a state of nonzero spin about its axis of symmetry.

The system is modeled as two rigid bodies in magnetostatic interaction: a ball with a magnetic dipole aligned to one of its axes, and a fixed magnetized ring of radially aligned magnetic dipoles. The main tool used to analyze the observed curious rotation is a Lagrange-Dirichlet stability criterion [16]. It is shown that the fixed points of the system’s governing equations correspond to the magnetic top being at rest with its axis of symmetry aligned with the local magnetic field and its translational position at a critical point of the magnetic potential energy. Stability of this point is determined by analyzing the nature of this critical point. If the attitude of the ring is normal to the surface, the magnetic potential energy is very nearly axisymmetric. A cross-sectional sketch of this potential energy is shown in Fig. 4.1. In this case there exists a ring of minima that are not individually stable. However, if the ring is tilted slightly, the potential has a unique local minimum opposite a saddle point as shown in the same figure.

If the ring is tilted and the ball’s initial position is unstable, the ball moves towards the stable fixed point which induces a resisting frictional force (see Fig. 4.2). The torque due to the sliding friction is in directions orthogonal to the moment arm \mathbf{q} . However, the torque due to the magnetic field counters the torques about the axes perpendicular to ξ_3 . This magnetic torque keeps ξ_3 aligned with the local magnetic field. Thus, the torque due to friction mainly causes a spin about the ξ_3 axis.

Thus far, the ring has been kept fixed. If the ring is perturbed slightly the position of

the local minimum will change. Hence this system is unstable with respect to perturbations of the ring. This instability will be utilized to design a prototype stochastic mechanical rectifier.

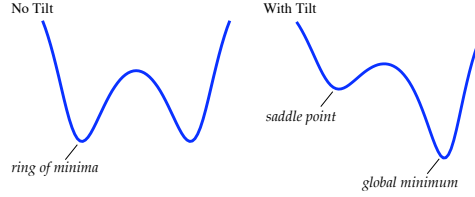


Figure 4.1: **Cross-Section of Potential Energy Surface.** Cross-sectional sketches of the magnetic potential energy with and without tilt. With no tilt in the ring, the potential energy surface is axisymmetric and has a ring of minima. If the ring is tilted slightly, a unique local minimum exists across from a saddle point.

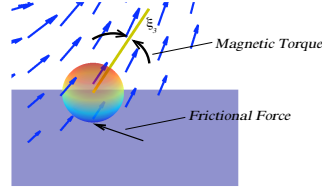


Figure 4.2: **Mechanism behind spin.** A sketch of the ball, its axis of symmetry ξ_3 , the ambient magnetic field (blue arrows), the restoring magnetic torques, and frictional force. The ball tends to a position that minimizes its potential energy. If the ball is initially unstable, then as it moves towards the minimum a frictional force resists this motion. The frictional force causes torques about axes orthogonal to the moment arm \mathbf{q} . However, the restoring magnetic torque counters the torques about the axes orthogonal to ξ_3 as shown in the sketch. This argument clarifies why the spin is primarily along ξ_3 .

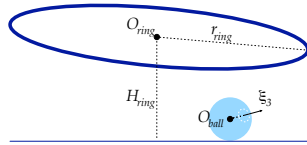


Figure 4.3: **Illustration of Magnetized Rigid Ball and Ring.** The figure depicts a rigid ball on a flat surface with a dipole fixed at the ball's centroid O_{ball} and in the direction ξ_3 . We will assume that the center of mass of the ball is coincident with O_{ball} . The ring is located at a height H_{ring} above a reference point O on the surface, and its radius is r_{ring} . The magnetic dipoles are placed symmetrically around this ring with dipole moments in the radial direction.

Hamel's magnetic top is modeled as an axisymmetric rigid ball of radius r and mass m . A magnetic dipole is attached to the center of mass, and in the direction of the axis of symmetry $\xi_3 \in \mathbb{R}^3$ as shown in Fig. 4.3. For simplicity, the surface friction is modelled using a sliding friction law. In what follows the continuous and discrete model are derived using the Hamilton-Pontryagin (HP) variational principle [3].

Magnetostatic Field Let $\mathbf{B} : \mathbb{R}^3 \rightarrow \mathbb{R}^3$ be the ambient magnetostatic field. For simplicity, we assume the magnetostatic field is due to a magnetic ring consisting of N magnetic

dipoles equally spaced around a ring of radius r_{ring} centered at the point O_{ring} and in the plane defined by the vector $\zeta_3 \in \mathbb{R}^3$. The point O_{ring} is at a height H_{ring} above a reference point O on the surface of the ball. To the reference point O , an orthonormal frame $(\mathbf{e}_x, \mathbf{e}_y, \mathbf{e}_z)$ is attached. For $i = 1, \dots, N$, let $\mathbf{d}_i \in \mathbb{R}^3$ denote the location of the i th-dipole with respect to O_{ring} and $\mathbf{m}_i \in \mathbb{R}^3$ denote its dipole moment. The dipole moments are assumed to be aligned in the radial direction of the ring. Let μ be the permeability of free space. The magnetic field of the i th-dipole at a field point $\mathbf{x} \in \mathbb{R}^3$ can be computed from the vector \mathbf{r}_i connecting the field point to the i th-dipole given by

$$\mathbf{r}_i = \mathbf{x} - r_{ring}\mathbf{d}_i - H_{ring}\mathbf{e}_z$$

using the standard formula for the magnetostatic field due to a dipole:

$$\mathbf{B}(\mathbf{r}_i, \mathbf{m}_i) = \frac{\mu}{4\pi\|\mathbf{r}_i\|^5} (3(\mathbf{r}_i^T \mathbf{m}_i)\mathbf{r}_i - \|\mathbf{r}_i\|^2 \mathbf{m}_i). \quad (4.1)$$

Using the principle of superposition, the magnetic field at a field point $\mathbf{x} \in \mathbb{R}^3$ due to the N dipoles is determined as the vector sum of the magnetic fields due to each dipole:

$$\mathbf{B}(\mathbf{x}) = \sum_{i=1}^N \mathbf{B}(\mathbf{r}_i, \mathbf{m}_i).$$

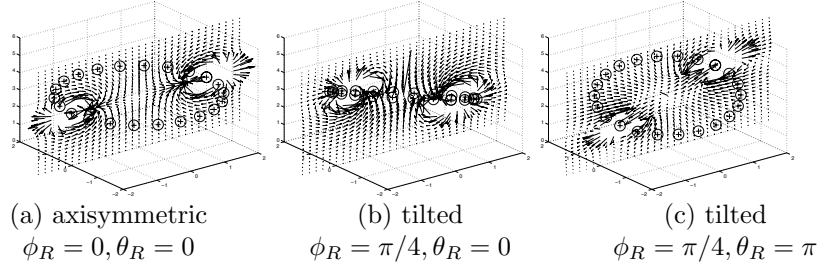


Figure 4.4: **Illustration of Magnetized Ring and its Magnetic Field.** The figures depict various orientations of a magnetized ring consisting of a discrete number of dipoles equally spaced around a circle in the plane defined by ζ_3 which is also depicted. The magnetic fields lines in the plane $y = 0$ are plotted. The angles ϕ_R and θ_R shown are the altitude and azimuth of the normal to the plane in which the ring is in. The height of the center of the ring, the radius of the ring, the number of dipoles, and the orientation of the ring are all parameters in this magnetostatic field model.

Lagrangian of Magnetic Ball The configuration space of the system is $Q = \mathbb{R}^3 \times \text{SO}(3)$ and its Lagrangian is denoted $L : TQ \rightarrow \mathbb{R}$. Let $(\mathbf{x}(t), \dot{\mathbf{x}}(t)) \in \mathbb{R}^3 \times \mathbb{R}^3$ denote the translational position and velocity of the ball measured with respect to the reference frame attached to O . Let $(\mathbf{e}_1, \mathbf{e}_2, \mathbf{e}_3)$ denote an inertial orthonormal frame attached to O_{ball} and related to a body-fixed frame (ξ_1, ξ_2, ξ_3) via the rotation matrix $R(t) \in \text{SO}(3)$. Let $J = \text{diag}(I_1, I_2, I_3)$ be the standard diagonal inertia matrix of the body and ξ_3 the axis of symmetry of the ball. We assume the mass distribution of the body is symmetric with respect to the axis of symmetry ξ_3 . This assumption implies that the principal moments of inertia about ξ_1 and ξ_2 are equal, i.e., $I = I_1 = I_2$. Let $(\mathbf{x}(t), \dot{\mathbf{x}}(t)) \in \mathbb{R}^3 \times \mathbb{R}^3$ denote the translational position and velocity of the ball.

We will use the isomorphism between \mathbb{R}^3 and the Lie algebra of $\text{SO}(3)$, $\mathfrak{so}(3)$, given by the hat map (See appendix.). In terms of this identification, we define the reduced Lagrangian

$\ell : \mathbb{R}^3 \times \mathbb{R}^3 \times \text{SO}(3) \times \mathbb{R}^3 \rightarrow \mathbb{R}$ as

$$\ell(\mathbf{x}, \dot{\mathbf{x}}, R, \boldsymbol{\omega}) = L(\mathbf{x}, \dot{\mathbf{x}}, R, \widehat{\boldsymbol{\omega}}R).$$

For the free magnetic ball, i.e., magnetic ball without dissipation, it is given explicitly by,

$$\ell(\mathbf{x}, \dot{\mathbf{x}}, R, \boldsymbol{\omega}) = \frac{m}{2} \dot{\mathbf{x}}^T \dot{\mathbf{x}} + \frac{1}{2} \boldsymbol{\omega}^T R J R^T \boldsymbol{\omega} - mg \mathbf{x}^T \mathbf{e}_3 + \boldsymbol{\xi}_3^T \mathbf{B}(\mathbf{x}). \quad (4.2)$$

From left the terms represent the translational and rotational kinetic energy of the ball, the gravitational potential energy and the dipole potential energy. The ball is also subject to the surface constraint $\varphi : \mathbb{R}^3 \rightarrow \mathbb{R}$ given by:

$$\varphi(\mathbf{x}) = -r + \mathbf{e}_3^T \mathbf{x}. \quad (4.3)$$

This holonomic constraint restricts the translational motion of the ball to a plane.

Governing Conservative Equations The equations of motion will be determined using a HP description [3]. The constrained HP action integral is given by,

$$s = \int_a^b \left[\ell(\mathbf{x}, \mathbf{v}, R, \boldsymbol{\omega}) + \langle \mathbf{p}, \dot{\mathbf{x}} - \mathbf{v} \rangle + \langle \widehat{\boldsymbol{\pi}}, \dot{R} R^T - \widehat{\boldsymbol{\omega}} \rangle + \lambda \varphi(\mathbf{x}) \right] dt.$$

The HP principle states that

$$\delta s = 0$$

where the variations are arbitrary except that the endpoints $(\mathbf{x}(a), R(a))$ and $(\mathbf{x}(b), R(b))$ are held fixed. The equations are given by,

$$\dot{\mathbf{x}} = \mathbf{v} \quad (\text{reconstruction equation}), \quad (4.4)$$

$$\mathbf{p} = \frac{\partial \ell}{\partial \mathbf{v}} \quad (\text{Legendre transform}), \quad (4.5)$$

$$\frac{d}{dt} \mathbf{p} = \frac{\partial \ell}{\partial \mathbf{x}} + \lambda \frac{\partial \varphi}{\partial \mathbf{x}} \quad (\text{Euler-Lagrange equations}), \quad (4.6)$$

$$\varphi(\mathbf{x}) = 0 \quad (\text{constraint equation}), \quad (4.7)$$

$$\frac{d}{dt} R = \widehat{\boldsymbol{\omega}} R \quad (\text{reconstruction equation}), \quad (4.8)$$

$$\boldsymbol{\pi} = \frac{\partial \ell}{\partial \boldsymbol{\omega}} \quad (\text{reduced Legendre transform}), \quad (4.9)$$

$$\frac{d}{dt} \widehat{\boldsymbol{\pi}} = \frac{\partial \ell}{\partial R} R^T - \widehat{\boldsymbol{\pi}} \widehat{\boldsymbol{\omega}} \quad (\text{Lie-Poisson equations}). \quad (4.10)$$

Evaluating these equations at ℓ as defined in (4.2) yields

$$\left\{ \begin{array}{lcl} \dot{\mathbf{x}} & = & \mathbf{v} \\ m \dot{\mathbf{v}} & = & (\mathbf{D}\mathbf{B}(\mathbf{x}))^T \boldsymbol{\xi}_3 + (\lambda - mg) \mathbf{e}_3 \\ \mathbf{x}^T \mathbf{e}_3 & = & r \\ \dot{R} & = & \widehat{\boldsymbol{\omega}} R \\ \boldsymbol{\pi} & = & R J R^T \boldsymbol{\omega} \\ \dot{\boldsymbol{\pi}} & = & \widehat{\boldsymbol{\xi}}_3 \mathbf{B}(\mathbf{x}). \end{array} \right. \quad (4.11)$$

Remark 4.1. Since the system is axisymmetric the Legendre transform in (4.11) simplifies:

$$\boldsymbol{\pi} = I\boldsymbol{\omega} + (I_3 - I)(\boldsymbol{\omega}^T \boldsymbol{\xi}_3)\boldsymbol{\xi}_3 \implies \boldsymbol{\omega} = \frac{1}{I} \left(\boldsymbol{\pi} + \frac{I - I_3}{I_3} (\boldsymbol{\pi}^T \boldsymbol{\xi}_3) \boldsymbol{\xi}_3 \right). \quad (4.12)$$

As a consequence one does not need to solve for the evolution of all three columns of $R(t)$ to integrate the ODE in $\boldsymbol{\pi}$. Instead one just needs to solve for the evolution of the third column, $\boldsymbol{\xi}_3$, using:

$$\dot{\boldsymbol{\xi}}_3 = \hat{\boldsymbol{\omega}} \boldsymbol{\xi}_3. \quad (4.13)$$

The following conservation law follows from axisymmetry.

Proposition 4.1. *The following momentum map is conserved under the flow of (4.11),*

$$J = \boldsymbol{\pi}^T \boldsymbol{\xi}_3.$$

Proof. This momentum map is due to an S^1 symmetry of the Lagrangian about the axis $\boldsymbol{\xi}_3$ which can be computed by formula (12.2.1) of [16]. The group acts on Q by:

$$\Phi_s^Q(\mathbf{x}, R) = (\mathbf{x}, \exp(s\hat{\boldsymbol{\xi}}_3)R).$$

The corresponding infinitesimal generator is given by:

$$\psi^Q(\mathbf{x}, R) = \frac{d}{ds} \Phi_s^Q(\mathbf{x}, R) \Big|_{s=0}.$$

Thus, one can invoke Noether's theorem to conclude the following momentum map $J : TQ \rightarrow (S^1)^*$ is preserved

$$J = \left\langle \frac{\partial L}{\partial \dot{R}}, \psi^Q(\mathbf{x}, R) \right\rangle = \frac{\partial \ell^T}{\partial \boldsymbol{\omega}} \boldsymbol{\xi}_3 = \boldsymbol{\pi}^T \boldsymbol{\xi}_3.$$

■

This conservation law indicates that if initially the top is not spinning about its axis of symmetry, then it will never spin about this axis. Thus, one cannot obtain the curious rotation using magnetic and gravitational effects alone. This result suggests surface friction will also play a role in producing this phenomenon.

Governing Nonconservative Equations Let $\mathbf{q} = -r\mathbf{e}_3$ denote the vector connecting the center of mass C to the contact point Q as shown in Fig. 4.3. We model the surface frictional force using a sliding friction law proportional to the slip velocity, i.e., the velocity of the contact point on the rigid body relative to the center of mass \mathbf{V}_Q :

$$\mathbf{F}_f = -c\mathbf{V}_Q$$

This law assumes zero static friction but, is nevertheless reasonable on very slippery surfaces where static friction is negligible. Moreover, it is an experimental fact that the magnetic top exhibits this curious rotation even on oily surfaces. In reality one must keep in mind that the ball is not in point-contact with the surface; rather, a finite area of the ball is in contact with the surface and is moving relative to the surface to make spinning possible. In this case this sliding model of friction is quite reasonable. A more refined model of friction would include rotational torque and dry frictional effects (Coulomb friction).

The slip velocity is given by:

$$\mathbf{V}_Q = \dot{\mathbf{x}} + \hat{\boldsymbol{\omega}} \mathbf{q}. \quad (4.14)$$

The force of friction is therefore,

$$\mathbf{F}_f = -c\mathbf{V}_Q,$$

and the torque due to friction is,

$$\boldsymbol{\tau}_f = \hat{\mathbf{q}}\mathbf{F}_f.$$

The governing dynamical equations of the magnetic ball with friction are given by:

$$\begin{cases} \dot{\mathbf{x}} &= \mathbf{v}, \\ m\dot{\mathbf{v}} &= (\mathbf{DB}(\mathbf{x}))^T \boldsymbol{\xi}_3 + (\lambda - mg)\mathbf{e}_3 - c(\mathbf{v} + r\hat{\mathbf{e}}_3\boldsymbol{\omega}), \\ \mathbf{x}^T \mathbf{e}_3 &= r, \\ \dot{\boldsymbol{\xi}}_3 &= \hat{\boldsymbol{\omega}}\boldsymbol{\xi}_3, \\ \boldsymbol{\omega} &= \frac{1}{I} \left(\boldsymbol{\pi} + \frac{I - I_3}{I_3} (\boldsymbol{\pi}^T \boldsymbol{\xi}_3) \boldsymbol{\xi}_3 \right), \\ \dot{\boldsymbol{\pi}} &= \hat{\boldsymbol{\xi}}_3 \mathbf{B}(\mathbf{x}) + cr\hat{\mathbf{e}}_3(\mathbf{v} + r\hat{\mathbf{e}}_3\boldsymbol{\omega}). \end{cases} \quad (4.15)$$

Remark 4.2. The fixed points of (4.15) satisfy:

$$\begin{aligned} \dot{\mathbf{x}} &= 0, \quad \boldsymbol{\omega} = 0 \\ \dot{\boldsymbol{\pi}} &= 0 \implies \boldsymbol{\xi}_3 = \kappa_2 \mathbf{B}(\mathbf{x}), \quad \kappa_2 \in \mathbb{R}, \text{ constant}, \\ \dot{\mathbf{v}} &= 0 \implies (\mathbf{DB}(\mathbf{x}))^T \mathbf{B}(\mathbf{x}) = 0. \end{aligned}$$

The Lagrange-Dirichlet criterion can be used to analyze the stability of these states since the kinetic energy vanishes at these fixed points and since the dissipation is proportional to velocity [16]. In particular, one can invoke a classical theorem due to Thomson-Tait-Chetaev, to conclude that if the fixed point is potentially stable or unstable, then it remains stable or unstable after introducing arbitrary dissipative forces proportional to velocities [17]. By this criterion, the fixed points are stable provided that the equilibrium is a strict local minimum of the potential energy. The potential energy evaluated at this equilibrium point is given by $V_e : \mathbb{R}^3 \rightarrow \mathbb{R}$,

$$V_e(\mathbf{x}) = -\kappa_2 \mathbf{B}(\mathbf{x})^T \mathbf{B}(\mathbf{x}).$$

In the limit as the number of dipoles along the ring is infinite, \mathbf{B} is axisymmetric with respect to the surface provided the attitude of the ring is normal to the surface on which the ball is on. In this case V_e can be written as a function of the distance to the origin: $f(\rho) = V_e(\mathbf{x})$ where $\rho = \|\mathbf{x}\|$ with $\mathbf{x}^T \mathbf{e}_3 = r$. Assume that the ring is above the ball and the potential energy is $V_e(\mathbf{x}) \leq 0$ for all $\mathbf{x} \in \mathbb{R}^3$. The origin is an unstable critical point, since f has a local maximum at that point. Moreover, $f(\rho)$ tends to zero as ρ becomes large. One can pick a distance $M \gg r_{ring}$ (the radius of the ring) sufficiently large to make $f(\rho)$ arbitrarily close to zero. In the interval $\rho \in (0, M)$, $V_e(\rho)$ is continuous, and therefore, the function has a local minimum in this interval. However, since f is axisymmetric this critical point is not a local minimum in the plane, but rather a circle of critical points. As shown in Fig. 4.5, the ball will be unstable with respect to circumferential perturbations. The figure also shows that when the axisymmetry of the magnetic field is broken by changing the orientation of the ring, there is a critical point that is a local minimum of $V_e(\mathbf{x})$.

Simulations Four simulations are performed on the top to confirm the theory and explain the curious rotation of the physical system. We use the HP integrator introduced in [3]. Let ϕ_B and θ_B denote the azimuth and altitude of the ball's attitude $\boldsymbol{\xi}_3$. In all of the simulations

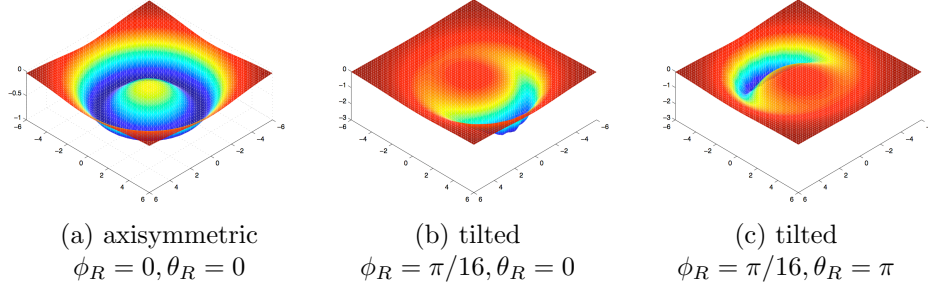


Figure 4.5: **Surface plot of V_e .** The potential energy surface is plotted as a function of x and y for ball radius $r = 0.3$, ring height $H = 2$, 25 dipoles on the ring, and ring radius $r_{ring} = 4$. The angles ϕ and θ shown are the altitude and azimuth of the normal to the plane in which the ring is in. By tilting the ring one can obtain a critical point which is a local minimum of V_e .

the top is initialized as follows:

$$\begin{aligned}
 c &= 0.1 \text{ kg} \cdot \text{m/s}, r = 1.8 \text{ cm}, m = 200 \text{ g}, \phi_B = 0, \theta_B = 0, I_3 = I_1 = 2/5mr^2, \\
 \mu \|\mathbf{m}_i\|/(4\pi) &= \mu \|\boldsymbol{\xi}_3\|/(4\pi) = 10^{-5} \text{ Tesla meter}^3, \\
 H_{ring} &= 20 \text{ cm}, N = 20 \text{ dipoles}, r_{ring} = 34 \text{ cm}
 \end{aligned}$$

The timestep size and number of timesteps are $h = 0.025$ and $N = 20000$ respectively. In the first four simulations the orientation of the ring is kept fixed. The first case simulated is when the magnetostatic field is axisymmetric and friction is absent. In this case the top undergoes what appears to be chaotic motion involving a balance between the magnetic potential and translational kinetic energies as shown in the simulation and Fig. 4.6. In the second simulation the altitude of the attitude of the ring is slightly perturbed causing the magnetostatic field to be noticeably asymmetric, see Fig. 4.7. However, in both of these cases the top does not acquire spin about the symmetry axis $\boldsymbol{\xi}_3$ as predicted by the theory.

In the presence of friction $c = 0.3$, the motion changes. The third case considered is the same configuration as the first case, but with friction. In this case the kinetic energy of the top is dissipated and the top moves towards a point where the magnetic potential energy is minimum, see Fig. 4.8. However, no spin develops. If the attitude of the ring is slightly perturbed, spin does develop as shown in Fig. 4.9. The origin of this spin in case 4 is explained here.

It is very clear from (4.15) that one can get spin about the axis of symmetry in the presence of friction. However, the frictional forces may produce torques about the other axes as well. So what is not clear is why the ball spins primarily about $\boldsymbol{\xi}_3$. This phenomenon is clarified in the following remark.

Remark 4.3. If the initial position of the ball is not a local minimum of the magnetic potential energy (as in the simulation), the position will be unstable as predicted by a Lagrange-Dirichlet criterion. The ball's position then adjusts to minimize its magnetic potential energy which causes sliding friction (see Fig. 4.2). The torque due to the sliding friction will introduce a torque in directions orthogonal to the moment arm \mathbf{q} . However, the torque due to the magnetic field will counter the torques about the axes perpendicular to $\boldsymbol{\xi}_3$. Keep in mind that the magnetic torque keeps $\boldsymbol{\xi}_3$ aligned with the local magnetic field. Thus, the torque due to friction mainly causes a spin about the $\boldsymbol{\xi}_3$ axis as shown in the simulation. Snapshots of the simulation are provided in Fig. 1.2.

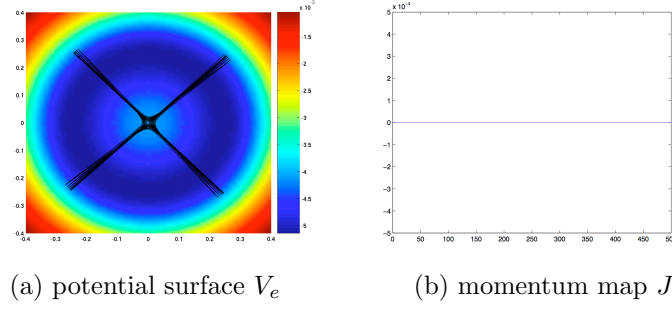


Figure 4.6: **Conservative Axisymmetric.** The figures plot $x(t), y(t)$ and $J(t)$ of the top in the absence of friction, and for $\phi_R = 0$ and $\theta_R = 0$. Superimposed on (a) is the potential energy level set which appears axisymmetric. (a) shows that the top bounces between the local maximum at the center and the circle of minima (dark blue ring). (b) shows that $J(t)$ is preserved as predicted by the theory. The accompanying simulation vividly illustrates this motion and demonstrates that one does not get curious rotation in this case.

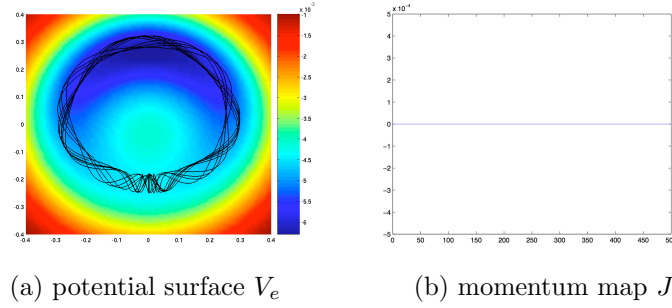


Figure 4.7: **Conservative Tilted.** The figures plot $x(t), y(t)$ and $J(t)$ of the top in the absence of friction, and for $\phi_R = 0$ and $\theta_R = \pi/64$. Superimposed on (a) is the potential energy level set which is no longer axisymmetric. (a) shows that the top moves erratically within an annulus. (b) confirms that $J(t)$ is preserved. The accompanying simulation vividly illustrates this motion and demonstrates that one does not get curious rotation in this case.

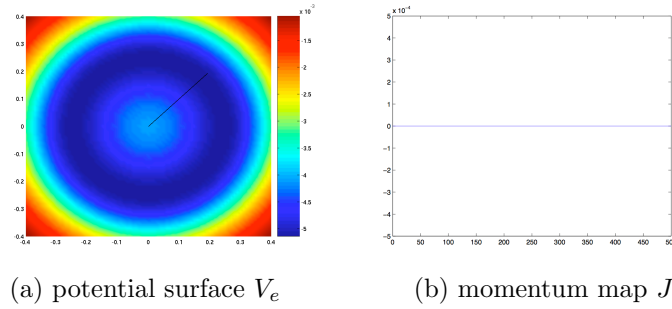


Figure 4.8: **Nonconservative Axisymmetric.** The figures plot $x(t), y(t)$ and $J(t)$ of the top in the presence of friction, and for $\phi_R = 0$ and $\theta_R = 0$. Superimposed on (a) is the potential energy level set which appears axisymmetric. (a) shows that the top moves from the local maximum at the center to a point that minimizes the potential energy (dark blue ring). However, (b) shows that no spin develops. The accompanying simulation vividly illustrates this motion and demonstrates that one does not get curious rotation in this case.

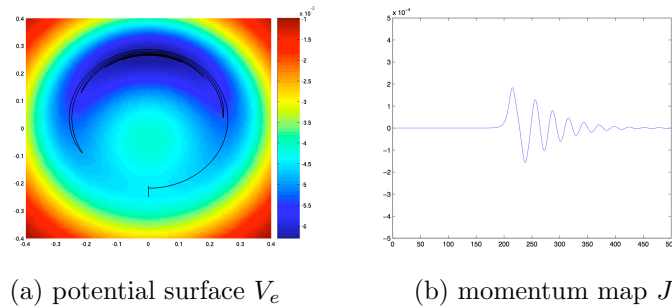


Figure 4.9: **Nonconservative Tilted.** The figures plot $x(t), y(t)$ and $J(t)$ of the top in the presence of friction, and for $\phi_R = 0$ and $\theta_R = \pi/64$. Superimposed on (a) is the potential energy level set which is no longer axisymmetric. (a) shows that the top moves along arcs. (b) confirms that one does get spin in this case. The accompanying simulation vividly illustrates this motion and clearly demonstrates that the ball goes from a state of rest to a state of nonzero spin about its attitude.

5 Fluctuation Driven Magnetic Motor

The instability of the top with respect to perturbations of the ring is the key idea behind the fluctuation driven magnetic motor. These random fluctuations are modelled as a white noise torque on the ring. However, if the ring is allowed to move freely, it could possibly turn on its side. To stabilize the ring, a fixed magnetized outer ring is installed.

By adjusting the radii and heights of the rings and the inertia of the inner ring, one can obtain a configuration in which the attitude of the inner ring can be randomly torqued without undergoing large excursions from the vertical position. In this case numerical experiments reveal that one can adjust the amplitude of the white noise so that the ball undergoes directed motion on certain time-scales. To be precise the numerics indicates that starting from a position of rest initially the top's motion is dominated by the effect of white noise. If the outer ring is close enough one can see the top oscillate between the wells in the magnetic potential caused by the dipoles in the outer ring. This behavior is reminiscent of stochastic resonance.

After some time, the top accumulates enough kinetic energy that it displays directed motion along a circle of certain radius. This motion is inertia-driven and the energy injected into the system by the white noise mainly adds to the speed of the top. Provided that the inner ring does not turn on its side, one of two things can happen: 1) the top reaches a critical velocity in which the amount of energy dissipated by the surface friction is on average equal to the amount of energy injected by the thermal noise or 2) the top gathers enough kinetic energy to escape from the potential well created by the inner and outer rings. Conducting this same experiment at uniform temperature, reveals that this phenomenon persists. The isothermal, magnetic ball-ring system is a prototype fluctuation-driven motor.

The fluctuation-driven motor considered in this paper is related to the granular, magnetic balls in ferrofluidic thermal ratchets. In such ratchets a time-varying magnetostatic field transfers angular momentum to magnetic spherical grains in a ferrofluid [8]. The ferromagnetic grains are modelled in the same way as the rigid ball in the prototype. However, our work is different in that the magnetic potential in the prototype is autonomous. In fact, the use of a non-autonomous potential to design a fluctuation driven motor is well understood [1].

In this section the equations of motion for the dynamics of a magnetic ball interacting with a dynamic, inner magnetized ring are derived. The magnetic effects of a fixed outer ring are also taken into account. As before the magnetic ball is assumed to be constrained to a

flat surface that resists the motion of the top via surface sliding friction. The center of mass of the inner ring is kept at a fixed height, but otherwise it is free to rotate and subjected to white noise torques. The governing stochastic differential equations are analyzed using energy arguments. Simulations validate this analysis and show that one can get sustained directed motion of the top from random perturbations of the inner ring. Moreover, it is shown that this phenomenon persists even when the system is at uniform temperature. This system is called a fluctuation driven magnetic motor.

The mass and radius of the magnetic ball are m and r respectively. The mass of the inner ring is m_{inner} . The heights and radii of the inner and outer rings are plotted and defined in Fig. 5.1.

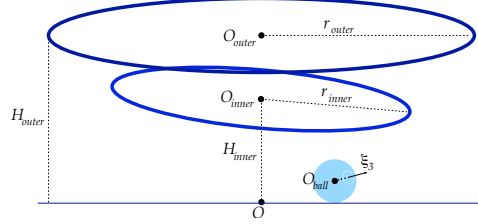


Figure 5.1: **Illustration of Magnetized Rings and Magnetic Top.** The figure shows the magnetic top on the surface with two rings above it. The inner and outer rings have radii r_{outer} and r_{inner} and heights H_{outer} and H_{inner} respectively. The centroids of the ball, inner and outer rings are also labeled. The purpose of the outer ring is to prevent the trivial equilibrium in which the inner ring turns on its side.

Lagrangian of Magnetic Ball & Inner Ring The configuration space of the system is $Q = \mathbb{R}^3 \times \text{SO}(3) \times \text{SO}(3)$. Let O_{ball} , O_{inner} and O_{outer} denote the centroids of the ball, inner and outer rings respectively. Let $(\mathbf{e}_1, \mathbf{e}_2, \mathbf{e}_3)$, $(\mathbf{f}_1, \mathbf{f}_2, \mathbf{f}_3)$, and $(\mathbf{g}_1, \mathbf{g}_2, \mathbf{g}_3)$ denote inertial orthonormal frames attached to O_{ball} , O_{inner} and O_{outer} , and related to body-fixed frames (ξ_1, ξ_2, ξ_3) , $(\zeta_1, \zeta_2, \zeta_3)$, and (η_1, η_2, η_3) via the rotation matrices $R_B(t)$, $R_R(t)$, and $R_O \in \text{SO}(3)$. Let $\mathbb{I}_B = \text{diag}(I_1, I_2, I_3)$ and $\mathbb{I}_R = \text{diag}(J_1, J_2, J_3)$ be the standard diagonal inertia matrices of the body and inner ring, and let ξ_3 and ζ_3 be the attitude of the ball and inner ring. The following assumptions are made: the outer ring is fixed, the mass distribution of the inner ring is symmetric with respect to its attitude (or axis of symmetry), and the ball's mass distribution is spherically symmetric. This assumption implies that $J_B = I_1 = I_2 = I_3$ and $J = J_1 = J_2$.

The magnetostatic field at any field point is due to the dipole in the ball, and an inner and outer ring consisting of N and M magnetic dipoles respectively. On each ring the dipoles are equally spaced around a circle of radius r_{inner} and r_{outer} in the planes defined by the vectors η_3 and $\zeta_3 \in \mathbb{R}^3$. We assume that there is no self-interaction between the dipoles within each body. The heights of the rings above the surface are denoted by H_{inner} and H_{outer} .

For $i = 1, \dots, N$ and $j = 1, \dots, M$, let $\mathbf{d}_i^{\text{inner}}(t)$ and $\mathbf{d}_j^{\text{outer}} \in \mathbb{R}^3$ denote the location of the i th and j th-dipoles on the inner and outer rings with respect to the points O_{inner} and O_{outer} and let $\mathbf{m}_i^{\text{inner}}(t)$ and $\mathbf{m}_j^{\text{outer}} \in \mathbb{R}^3$ denote the orientation of their respective dipole moments. The dipole moments are assumed to be in the radial direction of the ring. The magnetic field of each dipole at a field point can be determined from the vector \mathbf{r} connecting

the field point to the dipole using (4.1)

$$\begin{aligned}\mathbf{B}_i^{\text{inner}}(\mathbf{r}) &= \mathbf{B}(\mathbf{r}, \mathbf{m}_i^{\text{inner}}) \quad (\text{field of inner ring dipole}), \\ \mathbf{B}_j^{\text{outer}}(\mathbf{r}) &= \mathbf{B}(\mathbf{r}, \mathbf{m}_j^{\text{outer}}) \quad (\text{field of outer ring dipole}), \\ \mathbf{B}_0(\mathbf{r}) &= \mathbf{B}(\mathbf{r}, \boldsymbol{\xi}_3) \quad (\text{field of ball}).\end{aligned}$$

Define the following vectors $\mathbf{r}_{ij} \in \mathbb{R}^3$ $i = 0, \dots, N$ and $j = 0, \dots, M$ which joins the inner and outer dipoles, the inner dipoles to the ball, and outer dipoles to the ball as follows,

$$\mathbf{r}_{ij} = \begin{cases} -\mathbf{d}_j^{\text{outer}} - H_{\text{outer}}\mathbf{e}_3 + \mathbf{d}_i^{\text{inner}} + H_{\text{inner}}\mathbf{e}_3 & \text{if } i, j > 0 \quad (\text{ith outer to jth inner dipole}), \\ \mathbf{x} - \mathbf{d}_i^{\text{inner}} - H_{\text{inner}}\mathbf{e}_3 & \text{if } j = 0 \quad (\text{jth outer to ball}), \\ \mathbf{x} - \mathbf{d}_j^{\text{outer}} - H_{\text{outer}}\mathbf{e}_3 & \text{if } i = 0 \quad (\text{ith inner to ball}). \end{cases}$$

The spatial representation of the reduced Lagrangian $\ell : T\mathbb{R}^3 \times \text{SO}(3) \times \mathbb{R}^3 \times \text{SO}(3) \times \mathbb{R}^3 \rightarrow \mathbb{R}$ of the free magnetic ball, i.e., magnetic ball without dissipation, is given by,

$$\begin{aligned}\ell(\mathbf{x}, \dot{\mathbf{x}}, R_B, \boldsymbol{\omega}_B, R_R, \boldsymbol{\omega}_R) &= \frac{m}{2} \dot{\mathbf{x}}^T \dot{\mathbf{x}} + \frac{1}{2} J_B \boldsymbol{\omega}_B^T \boldsymbol{\omega}_B + \frac{1}{2} \boldsymbol{\omega}_R^T R_R \mathbb{I}_R R_R^T \boldsymbol{\omega}_R \\ &+ 2 \sum_{i=1}^N \boldsymbol{\xi}_3^T \mathbf{B}_i^{\text{inner}}(\mathbf{r}_{i0}) + \sum_{j=1}^M \boldsymbol{\xi}_3^T \mathbf{B}_j^{\text{outer}}(\mathbf{r}_{0j}) + \sum_{i=1}^N \sum_{j=1}^M (\mathbf{m}_i^{\text{inner}})^T \mathbf{B}_j^{\text{outer}}(\mathbf{r}_{ij})\end{aligned} \quad (5.1)$$

From left the terms represent the translational and rotational kinetic energy of the ball, the rotational kinetic energy of the ring, the gravitational potential energy of the ball and the magnetic potential energy of the inner ring and ball dipoles.

Governing Equations for Magnetic Ball & Ring The equations of motion are determined from a Hamilton-Pontryagin (HP) principle [3]. The HP action integral is given by,

$$s = \int_a^b \left[\ell(\mathbf{x}, \dot{\mathbf{x}}, R_B, \boldsymbol{\omega}_B, R_R, \boldsymbol{\omega}_R) + \left\langle \widehat{\boldsymbol{\pi}}_B, \dot{R}_B R_B^T - \widehat{\boldsymbol{\omega}}_B \right\rangle + \left\langle \widehat{\boldsymbol{\pi}}_R, \dot{R}_R R_R^T - \widehat{\boldsymbol{\omega}}_R \right\rangle + \lambda \varphi(\mathbf{x}) \right] dt.$$

The HP principle states that

$$\delta s = 0$$

where the variations are arbitrary except that the endpoints $(\mathbf{x}(a), R_B(a), R_R(a))$ and $(\mathbf{x}(b), R_B(b), R_R(b))$ are held fixed. The equations are given by,

$$\frac{d}{dt} \frac{\partial \ell}{\partial \dot{\mathbf{x}}} = \frac{\partial \ell}{\partial \mathbf{x}} + \lambda \frac{\partial \varphi}{\partial \mathbf{x}} \quad (\text{Euler-Lagrange equations for ball}), \quad (5.2)$$

$$\varphi(\mathbf{x}) = 0 \quad (\text{constraint equation}), \quad (5.3)$$

$$\frac{d}{dt} R_B = \widehat{\boldsymbol{\pi}}_B R_B \quad (\text{reconstruction equation for ball}), \quad (5.4)$$

$$\frac{d}{dt} R_R = \widehat{\boldsymbol{\pi}}_R R_R \quad (\text{reconstruction equation for ring}), \quad (5.5)$$

$$\boldsymbol{\pi}_B = \frac{\partial \ell}{\partial \boldsymbol{\omega}_B} \quad (\text{reduced Legendre transform for ball}), \quad (5.6)$$

$$\boldsymbol{\pi}_R = \frac{\partial \ell}{\partial \boldsymbol{\omega}_R} \quad (\text{reduced Legendre transform for ring}), \quad (5.7)$$

$$\frac{d}{dt} \widehat{\boldsymbol{\pi}}_B = \frac{\partial \ell}{\partial R_B} R_B^T - \widehat{\boldsymbol{\pi}}_B \boldsymbol{\omega}_B \quad (\text{Lie-Poisson equations for ball}), \quad (5.8)$$

$$\frac{d}{dt} \widehat{\boldsymbol{\pi}}_R = \frac{\partial \ell}{\partial R_R} R_R^T - \widehat{\boldsymbol{\pi}}_R \boldsymbol{\omega}_R \quad (\text{Lie-Poisson equations for ring}). \quad (5.9)$$

The nonconservative system is obtained by adding the frictional force and torque derived earlier to the translational and rotational equations of the ball: (5.2) and (5.8).

Random Perturbations & Uniform Temperature Consider driving the inner ring by the following Wiener process. Let $\mathbf{W} \in \mathbb{R}^3$ denote Brownian motion in \mathbb{R}^3 , and append the following random torque:

$$\mathbf{T}_R = \alpha d\mathbf{W} \in \mathbb{R}^3$$

to the Lie-Poisson equation for the ring (5.9).

The work performed by \mathbf{T}_R is equal to the change in total energy of the system. On the other hand, the work done by the kicks over a time interval $[a, b]$ is given by the following formula:

$$\text{Work of kicks} = \alpha \int_a^b \mathbf{T}_R^T \boldsymbol{\omega}_R. \quad (5.10)$$

The work transferred from the inner ring to the top is given by:

$$\text{Work transferred to top} = \Delta \text{Total Energy} - \Delta \text{Ring Energy}. \quad (5.11)$$

Thus a measure of the efficiency of the magnetic motor is given by the following ratio:

$$\text{Efficiency} = \frac{\text{Work transferred to top}}{\text{Work of kicks}}. \quad (5.12)$$

As a next step frictional torque is introduced to the inner ring and thermal torque (white noise) to the ball, so that the generator of the process is characterized by a unique Gibbs-Boltzmann invariant distribution. The reader is referred to the Appendix for the governing equations of the magnetic motor at uniform and non-uniform temperatures.

Simulations A stochastic variational integrator is used to carry out these simulations [5]. Simulations are conducted at uniform and non-uniform temperature as described below. The initial conditions and parameters used are given by

$$\begin{aligned} c &= 0.15 \text{ kg} \cdot \text{m/s}, r = 4.0 \text{ cm}, m = 500 \text{ g}, \phi_B = 0, \theta_B = 0, I_3 = I_1 = 2/5mr^2, \\ \mu \|\mathbf{m}_i^{\text{inner, outer}}\|/(4\pi) &= \mu \|\boldsymbol{\xi}_3\|/(4\pi) = 2 \times 10^{-6} \text{ T} \cdot \text{m}^3, \\ H_{\text{inner}} = H_{\text{outer}} &= 48 \text{ cm}, N = 20 \text{ dipoles}, M = 5 \text{ dipoles}, \\ r_{\text{inner}} = 75 \text{ cm}, r_{\text{outer}} &= 98 \text{ cm}, m_{\text{inner}} = 6 \text{ kg}, J_3 = m_{\text{inner}}r_{\text{inner}}^2, J = 1/2J_3. \end{aligned}$$

In all of the simulations the magnetic top is initially at rest with its attitude aligned to the vertical. The difference in the simulations is the amplitude of the oscillations and the discrete sample from the normal distribution. Figures 5.6-2.2 present data from the uniform temperature simulations. The key point about the uniform temperature simulations is as seen in Figures 5.9 and 2.2 the magnetic top transitions from noise to ballistic motion. As expected the non-uniform temperature case also exhibits this behavior as shown in Figures 5.2-2.1.

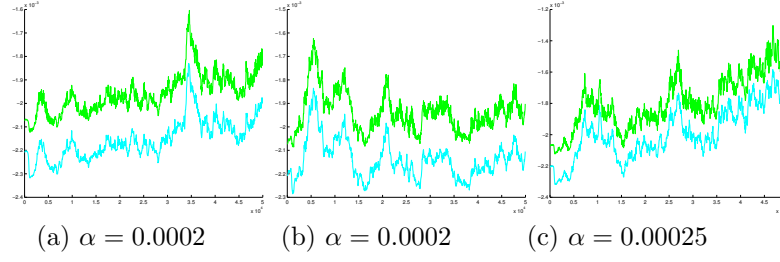


Figure 5.2: **Total and inner ring energy (non-uniform temperature)**. The total energy of the system is shown in green and the ring energy in cyan for different amplitudes of the noise and for two different samples. Although there is dissipation, the thermal fluctuations inject energy into the system.

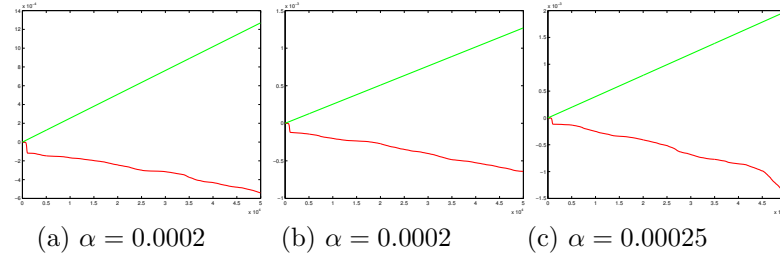


Figure 5.3: **Energy injected and dissipated (non-uniform temperature)**. A plot of the energy injected by the white noise as computed analytically and dissipated by friction computed numerically.

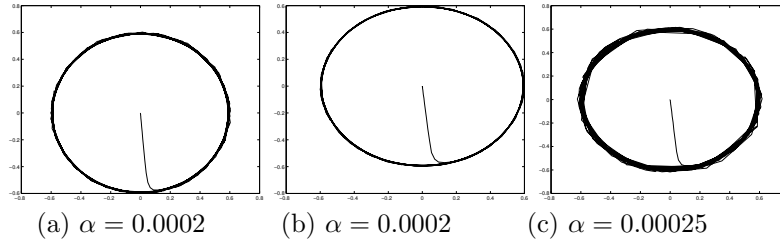


Figure 5.4: **xy-position of magnetic ball (non-uniform temperature)**. An aerial view of the path of the center of mass of the ball in the xy-plane.

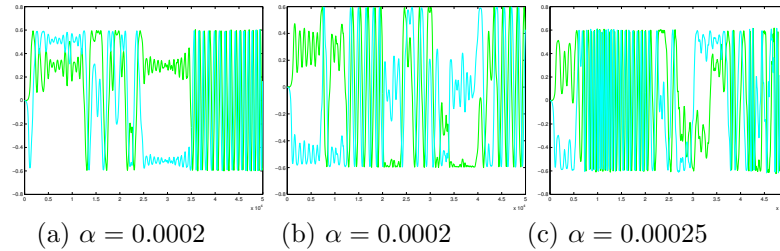


Figure 5.5: **xy-position of magnetic ball planar view (non-uniform temperature)**. The x and y components of the center of mass are plotted in green and blue respectively. It is very clear from this plot that the motion transitions from noise driven to being inertia driven.

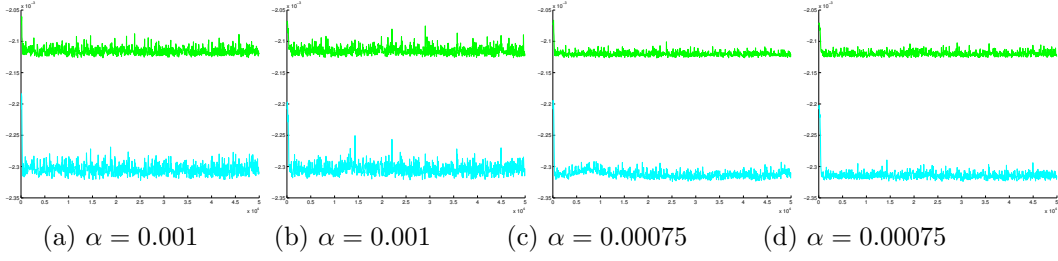


Figure 5.6: **Total and inner ring energy (uniform temperature).** The total energy of the system is shown in green and the ring energy in cyan for different amplitudes of the noise. Although there is dissipation, the thermal fluctuations inject energy into the system.

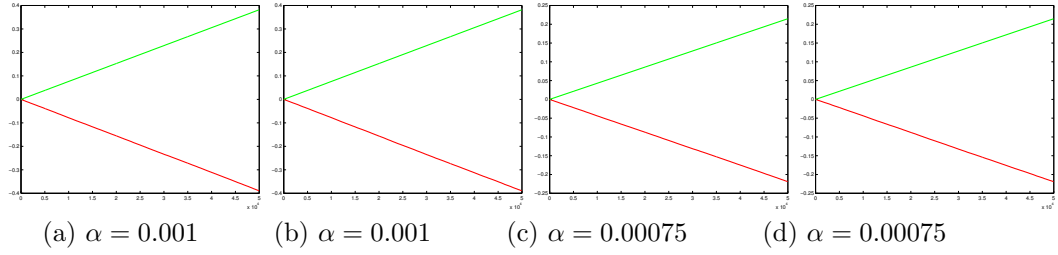


Figure 5.7: **Energy injected and dissipated (uniform temperature).** A plot of the energy injected by the white noise as computed analytically and dissipated by friction computed numerically. In the constant temperature case we see an approximate balance between these energies.

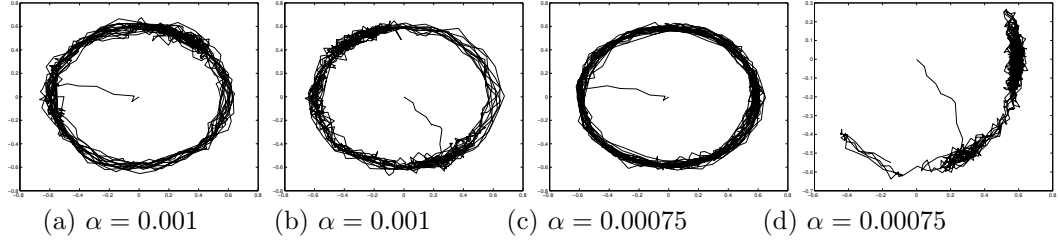


Figure 5.8: **xy-position of magnetic ball (uniform temperature).** An aerial view of the path of the center of mass of the ball in the xy-plane.

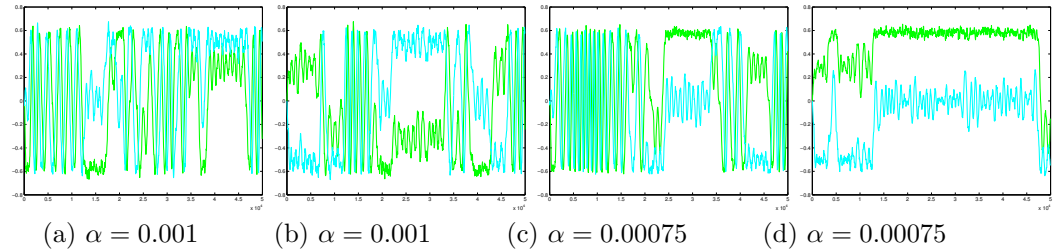


Figure 5.9: **xy-position of magnetic ball planar view (uniform temperature).** The x and y components of the center of mass are plotted in green and blue respectively. It is very clear from this plot that the motion transitions from noise driven to being inertia driven.

6 Conclusion

This paper introduces a novel mechanism to rectify random perturbations to achieve directed motion as a meta-stable state and ballistic mean-squared displacement with respect to the invariant law. The basic idea behind the mechanism is explained using the simple sliding disk model. With this model one can prove that if the potential energy is non-constant, then the invariant Gibbs measure of the system, μ , is ergodic and strongly mixing. As a consequence μ a.s. it is shown that the translational displacement of the sliding disk is not ballistic. However, it is shown that the mean-squared displacement with respect to the invariant law is ballistic.

This anomalous diffusion manifests itself numerically. That is, starting from a position at rest and when U is non-constant, one observes flights in the x -displacement over time-scales which are random and the probability distribution of the flight-durations have a heavy tail. Moreover, from a numerical statistical analysis, it is observed that the mean-squared translational displacement of the sliding disk is ballistic and its translational displacement is characterized by long time memory/correlation. The paper proceeds to show that this basic phenomenon arises in a more complex, rigid-body system consisting of two rigid bodies interacting via magnetostatic effects. Along the way we explain the observed dynamics of Hamel's magnetic device.

7 Appendix

SO(3) Preliminaries In the paper we use the following isomorphism between an element of the Lie algebra of $\text{SO}(3)$, $T_e \text{SO}(3) = \mathfrak{so}(3)$, and \mathbb{R}^3 . Recall that elements of $\mathfrak{so}(3)$ are skew-symmetric matrices with Lie bracket given by the matrix commutator. Let $\boldsymbol{\omega} = (\omega_1, \omega_2, \omega_3)$. Then one can relate \mathbb{R}^3 with a skew-symmetric matrix via the hat map $\hat{\cdot}: \mathbb{R}^3 \rightarrow \mathfrak{so}(3)$,

$$\hat{\boldsymbol{\omega}} = \begin{bmatrix} 0 & -\omega_3 & \omega_2 \\ \omega_3 & 0 & -\omega_1 \\ -\omega_2 & \omega_1 & 0 \end{bmatrix}.$$

Let $g(t)$ be a curve in $\text{SO}(3)$. With this identification of $\mathfrak{so}(3)$ to \mathbb{R}^3 , the right-trivialization of a tangent vector \dot{g} to this curve, given by $\xi = TR_{g^{-1}} \cdot \dot{g} \in \mathfrak{so}(3)$, can be written in terms of the spatial angular velocity vector $\boldsymbol{\omega} \in \mathbb{R}^3$, i.e., as $\xi = \hat{\boldsymbol{\omega}} \in \mathfrak{so}(3)$.

Magnetic motor at non-uniform temperature governing equations Below the governing equations of the ring-ball system with nonconservative effects due to surface friction and white noise are written in Ito form. We introduce the potential energy function $U: \mathbb{R}^3 \times \text{SO}(3) \times \text{SO}(3) \rightarrow \mathbb{R}$ which represents the total potential energy of the ring-ball

system. In terms of U the governing equations can be written as,

$$\begin{aligned}
d\mathbf{x} &= \mathbf{v}dt \\
d\mathbf{v} &= \frac{1}{m} \left(-\frac{\partial U}{\partial \mathbf{x}} + (\lambda - mg)\mathbf{e}_3 - c\mathbf{V}_Q \right) dt \\
\mathbf{x}^T \mathbf{e}_3 &= r \\
dR_B &= \widehat{\boldsymbol{\omega}}_B R_B dt \\
dR_R &= \widehat{\boldsymbol{\omega}}_R R_R dt \\
\boldsymbol{\pi}_B &= J_B \boldsymbol{\omega}_B \\
\boldsymbol{\pi}_R &= R_R \mathbb{I}_R R_R^T \boldsymbol{\omega}_R \\
d\widehat{\boldsymbol{\pi}}_B &= \left(-\frac{\partial U}{\partial R_B} R_B^T - c\widehat{\mathbf{q}}\mathbf{V}_Q \right) dt \\
d\widehat{\boldsymbol{\pi}}_R &= \left(-\frac{\partial U}{\partial R_R} R_R^T \right) dt + \alpha d\widehat{\mathbf{W}}
\end{aligned}$$

Evaluating these governing equations at ℓ defined in (5.1) yields

$$d\mathbf{x} = \mathbf{v}dt \quad (7.1)$$

$$\begin{aligned}
d\mathbf{v} &= \frac{1}{m} \left(2 \sum_{i=1}^N \mathbf{D}\mathbf{B}_i^{\text{inner}}(\mathbf{r}_{i0})^T \boldsymbol{\xi}_3 + \sum_{j=1}^M \mathbf{D}\mathbf{B}_j^{\text{outer}}(\mathbf{r}_{0j})^T \boldsymbol{\xi}_3 \right) dt \\
&\quad + \frac{1}{m} (-c\mathbf{V}_Q + (\lambda - mg)\mathbf{e}_3) dt
\end{aligned} \quad (7.2)$$

$$\mathbf{x}^T \mathbf{e}_3 = r \quad (7.3)$$

$$dR_B = \widehat{\boldsymbol{\omega}}_B R_B dt \quad (7.4)$$

$$dR_R = \widehat{\boldsymbol{\omega}}_R R_R dt \quad (7.5)$$

$$\boldsymbol{\pi}_B = J_B \boldsymbol{\omega}_B \quad (7.6)$$

$$\boldsymbol{\pi}_R = R_R \mathbb{I}_R R_R^T \boldsymbol{\omega}_R \quad (7.7)$$

$$d\boldsymbol{\pi}_B = \widehat{\boldsymbol{\xi}}_3 \left(2 \sum_{i=1}^N \mathbf{B}_i^{\text{inner}}(\mathbf{r}_{i0}) + \sum_{j=1}^M \mathbf{B}_j^{\text{outer}}(\mathbf{r}_{0j}) \right) dt - c\widehat{\mathbf{q}}\mathbf{V}_Q dt, \quad (7.8)$$

$$\begin{aligned}
d\boldsymbol{\pi}_R &= 2 \sum_{i=1}^N \left[\widehat{\mathbf{m}}_i^{\text{inner}} \mathbf{B}_0(\mathbf{r}_{i0}) - \widehat{\mathbf{d}}_i^{\text{inner}} (\mathbf{D}\mathbf{B}_i^{\text{inner}}(\mathbf{r}_{i0})^T \boldsymbol{\xi}_3) \right] dt \\
&\quad + \sum_{i=1}^N \sum_{j=1}^M \left[\widehat{\mathbf{m}}_i^{\text{inner}} \mathbf{B}_j^{\text{outer}}(\mathbf{r}_{ij}) + \widehat{\mathbf{d}}_i^{\text{inner}} (\mathbf{D}\mathbf{B}_j^{\text{outer}}(\mathbf{r}_{ij})^T \mathbf{m}_i^{\text{inner}}) \right] dt \\
&\quad + \alpha d\widehat{\mathbf{W}}.
\end{aligned} \quad (7.9)$$

Since the ring is axisymmetric its Legendre transform simplifies:

$$\boldsymbol{\pi}_R = J\boldsymbol{\omega}_R + (J_3 - J)(\boldsymbol{\omega}_R^T \boldsymbol{\zeta}_3)\boldsymbol{\zeta}_3 \implies \boldsymbol{\omega}_R = \frac{1}{J} \left(\boldsymbol{\pi}_R + \frac{J - J_3}{J_3} (\boldsymbol{\pi}_R^T \boldsymbol{\zeta}_3) \boldsymbol{\zeta}_3 \right). \quad (7.10)$$

Remark 7.1. The energy of the magnetic motor is given by

$$E(\mathbf{x}, \mathbf{v}, R_B, \boldsymbol{\pi}_B, R_R, \boldsymbol{\pi}_R) = \frac{m}{2} \mathbf{v}^T \mathbf{v} + \frac{1}{2} J_B^{-1} \boldsymbol{\pi}_B^T \boldsymbol{\pi}_B + \frac{1}{2} \boldsymbol{\pi}_R^T R_R \mathbb{I}_R^{-1} R_R^T \boldsymbol{\pi}_R + U(\mathbf{x}, R_B, R_R).$$

Using Ito's formula one can calculate the stochastic differential of the energy in the case when the magnetic motor is at non-uniform temperature

$$dE = \left(-c \mathbf{V}_Q^T \mathbf{V}_Q + \frac{1}{2} \alpha^2 \text{trace} [\mathbb{I}_R^{-1}] \right) dt + \alpha \boldsymbol{\omega}_R^T d\mathbf{W}.$$

Integrating yields,

$$E(t) - E(0) = -c \int_0^t \mathbf{V}_Q^T \mathbf{V}_Q ds + \frac{1}{2} \alpha^2 \text{trace} [\mathbb{I}_R^{-1}] t + \text{martingales}.$$

The first term represents the energy dissipated by friction. The next terms represent the work done by the white noise torque as computed by Ito's integral.

Isothermal, magnetic motor governing equations Similar to the sliding disk, to put the magnetic motor at constant temperature we define the following dissipation matrix,

$$\mathbf{C} = \begin{bmatrix} 1/m^2 & 0 & 0 & -r/(mJ) \\ 0 & 1/m^2 & r/(mJ) & 0 \\ 0 & r/(mJ) & r^2/J^2 & 0 \\ -r/(mJ) & 0 & 0 & r^2/J^2 \end{bmatrix}$$

The translational position of the ball is written in coordinates as $\mathbf{x} = (x_1, x_2, r)$. The translational and angular velocities of the ball are given by $\mathbf{v} = (v_1, v_2, 0)$ and $\boldsymbol{\omega}_B = (\omega_B^{(1)}, \omega_B^{(2)}, \omega_B^{(3)})$. The dynamical equations for the constant temperature magnetic motor are given by:

$$dx_1 = v_1 dt \quad (7.11)$$

$$dx_2 = v_2 dt \quad (7.12)$$

$$dR_B = \widehat{\boldsymbol{\omega}}_B R_B dt \quad (7.13)$$

$$dR_R = \widehat{\boldsymbol{\omega}}_R R_R dt \quad (7.14)$$

$$\begin{bmatrix} dv_1 \\ dv_2 \\ d\omega_B^{(1)} \\ d\omega_B^{(2)} \end{bmatrix} = - \begin{bmatrix} U_x^T \mathbf{e}_1 / m \\ U_x^T \mathbf{e}_2 / m \\ U_B^T \mathbf{e}_1 / J \\ U_B^T \mathbf{e}_2 / J \end{bmatrix} dt - c_B \mathbf{C} \begin{bmatrix} mv_1 \\ mv_2 \\ J\omega_B^{(1)} \\ J\omega_B^{(2)} \end{bmatrix} + \alpha_B \mathbf{C}^{1/2} \begin{bmatrix} dB_{v_1} \\ dB_{v_2} \\ dB_{\omega_B^{(1)}} \\ dB_{\omega_B^{(2)}} \end{bmatrix} \quad (7.15)$$

$$d\omega_B^{(3)} = -U_B^T \mathbf{e}_3 / J \quad (7.16)$$

$$\boldsymbol{\pi}_R = R_R \mathbb{I}_R R_R^T \boldsymbol{\omega}_R \quad (7.17)$$

$$d\boldsymbol{\pi}_R = -U_R - c_R \boldsymbol{\omega}_R + \alpha_R d\mathbf{B}_R \quad (7.18)$$

The terms U_x , U_B , and U_R are defined in terms of the inner product on \mathbb{R}^3 as,

$$U_x^T y = \left\langle \frac{\partial U}{\partial x}, y \right\rangle = \partial_x U(x, R_B, R_R) \cdot y$$

$$U_B^T y = \left\langle \frac{\partial U}{\partial R_B} R_B^T, \hat{y} \right\rangle = \partial_{R_B} U(x, R_B, R_R) \cdot \hat{y} R_B$$

$$U_R^T y = \left\langle \frac{\partial U}{\partial R_R} R_R^T, \hat{y} \right\rangle = \partial_{R_R} U(x, R_B, R_R) \cdot \hat{y} R_R$$

and $\partial_{R_B} U, \partial_{R_R} U : \text{SO}(3) \rightarrow T_R^* \text{SO}(3)$, and $\partial_x U : \mathbb{R}^3 \rightarrow T_x^* \mathbb{R}^3$. Similar to the sliding disk at uniform temperature, one can prove the following.

Theorem 7.1. *Let χ denote the phase space of the magnetic motor. Set ξ to be the solution of (7.11)-(7.18). Suppose that $c_R/\alpha_R^2 = c_B/\alpha_B^2$. Let E denote the energy of the magnetic motor given by,*

$$E(\mathbf{x}, \mathbf{v}, R_B, \boldsymbol{\pi}_B, R_R, \boldsymbol{\pi}_R) = \frac{m}{2} \mathbf{v}^T \mathbf{v} + \frac{1}{2} J_B^{-1} \boldsymbol{\pi}_B^T \boldsymbol{\pi}_B + \frac{1}{2} \boldsymbol{\pi}_R^T R_R \mathbb{I}_R^{-1} R_R^T \boldsymbol{\pi}_R + U(\mathbf{x}, R_B, R_R).$$

Let $\beta = 2c_B/\alpha_B^2$. The following measure,

$$\mu(d\xi) := \frac{e^{-\beta E}}{Z} d\xi \quad (7.19)$$

is the unique Gibbs invariant measure of the stochastic process ξ .

Remark 7.2. By using Ito's formula one can show that:

$$dE = \left(-c_B \mathbf{V}_Q^T \mathbf{V}_Q - c_R \boldsymbol{\omega}_R^T \boldsymbol{\omega}_R + \alpha_B^2 \left(\frac{1}{m} + \frac{r^2}{J} \right) dt + \frac{1}{2} \alpha_R^2 \text{trace} [\mathbb{I}_R^{-1}] \right) dt + \text{martingales}.$$

Integrating yields,

$$\begin{aligned} E(t) - E(0) = & -c_B \int_0^t \mathbf{V}_Q^T \mathbf{V}_Q ds - c_R \int_0^t \boldsymbol{\omega}_R^T \boldsymbol{\omega}_R ds \\ & + \alpha_B^2 \left(\frac{1}{m} + \frac{r^2}{J} \right) t + \frac{1}{2} \alpha_R^2 \text{trace} [\mathbb{I}_R^{-1}] t + \text{martingales}. \end{aligned}$$

References

- [1] A. Ajdari and J. Prost. Drift induced by a periodic potential of low symmetry: pulsed dielectrophoresis. *C. R. Acad. Sci. Paris II*, 315:1635–1639, 1992.
- [2] R. Dean Astumian. Thermodynamics and kinetics of a brownian motor. *Science*, 276(5314):917 – 922, 1997.
- [3] N. Bou-Rabee and J. E. Marsden. Hamilton-pontryagin integrators on lie groups part i: Introduction and structure-preserving properties. Submitted; arXiv:, 2007.
- [4] N. Bou-Rabee and H. Owhadi. Ergodicity for langevin processes with degenerate diffusion in momentums. Submitted; arXiv:, 2007.
- [5] N. Bou-Rabee and H. Owhadi. Stochastic variational integrators. Submitted; arXiv:0708.2187, 2007.
- [6] R. W. Brockett. On the rectification of vibratory motion. *Sensors and Actuators*, 20:91–96, 1989.
- [7] S. Ciliberto and C. Laroche. An experimental test of the gallavotti-cohen fluctuation theorem. *J. Phys. IV*, 8(P6):215–219, OCT 1998.
- [8] A. Engel, H. W. Muller, P. Riemann, and A. Jung. Ferrofluids as thermal ratchets. *Physical Review Letters*, 91(6):060602, 2003.
- [9] V. Y. Frenkel. On the history of the einstein de haas effect. *Sov. Phys. Uspekhi*, 22(7):580–587, 2007.
- [10] G. Gallavotti and E. G. D. Cohen. Dynamical ensembles in nonequilibrium statistical-mechanics. *Phys. Rev. Lett.*, 74(14):2694–2697, APR 1995.
- [11] H. Gernsback. Tesla’s egg of colombus: How tesla performed the feat of colombus without cracking the egg. *Electrical Experimenter*, 808:774–775, 2007. See as well <http://www.tfcbooks.com/articles/tac2.htm>.
- [12] Joel L. Lebowitz and Herbert Spohn. A Gallavotti-Cohen-type symmetry in the large deviation functional for stochastic dynamics. *J. Statist. Phys.*, 95(1-2):333–365, 1999.
- [13] M. Liao. Random motion of a rigid body. *Journal of Theoretical Probability*, 10(1):201–211, 1997.
- [14] M. Liao and L. Wang. Motion of a rigid body under random perturbation. *Electronic Communications in Probability*, 10:235–243, 2005.
- [15] J. Manning and P. Sinclair. The granite man and the butterfly. *Fort Langley, B.C., Canada: Project Magnet Inc.*, 1995. See as well <http://jnaudin.free.fr/html/hamspin.htm>.
- [16] J. E. Marsden and T. Ratiu. *Introduction to Mechanics and Symmetry*. Springer Texts in Applied Mathematics, 1999.
- [17] D. R. Merkin. *Introduction to the Theory of Stability*. Springer, 2002.
- [18] G. Da Prato and J. Zabczyk. *Ergodicity for Infinite Dimensional Systems*. Cambridge University Press, 1996.

- [19] Peter Reimann. Brownian motors: noisy transport far from equilibrium. *Physics Reports*, 361(2-4):57–265, 2002.
- [20] G. M. Wang, E. M. Sevick, E. Mittag, D. J. Searles, and D. J. Evans. Experimental demonstration of violations of the second law of thermodynamics for small systems and short time scales. *Physical Review Letters*, 89(5):050601, 2002.